Author Manuscript

Author Manuscript

Author Manuscript

Author Manuscript

HHS Public Access

Author manuscript

*Int J Coal Geol*. Author manuscript; available in PMC 2015 October 01.

Published in final edited form as:

*Int J Coal Geol*. 2013 July 30; 114: 96–113. doi:10.1016/j.coal.2013.02.011.

# Integration of vertical and in-seam horizontal well production analyses with stochastic geostatistical algorithms to estimate pre-mining methane drainage efficiency from coal seams: Blue Creek seam, Alabama

**C. Özgen Karacan***

NIOSH, Office of Mine Safety and Health Research, Pittsburgh, PA 15236, United States

## Abstract

Coal seam degasification and its efficiency are directly related to the safety of coal mining. Degasification activities in the Black Warrior basin started in the early 1980s by using vertical boreholes. Although the Blue Creek seam, which is part of the Mary Lee coal group, has been the main seam of interest for coal mining, vertical wellbores have also been completed in the Pratt, Mary Lee, and Black Creek coal groups of the Upper Pottsville formation to degasify multiple seams. Currently, the Blue Creek seam is further degasified 2–3 years in advance of mining using in-seam horizontal boreholes to ensure safe mining.

The studied location in this work is located between Tuscaloosa and Jefferson counties in Alabama and was degasified using 81 vertical boreholes, some of which are still active. When the current long mine expanded its operation into this area in 2009, horizontal boreholes were also drilled in advance of mining for further degasification of only the Blue Creek seam to ensure a safe and a productive operation. This paper presents an integrated study and a methodology to combine history matching results from vertical boreholes with production modeling of horizontal boreholes using geostatistical simulation to evaluate spatial effectiveness of in-seam boreholes in reducing gas-in-place (GIP).

Results in this study showed that in-seam wells' boreholes had an estimated effective drainage area of 2050 acres with cumulative production of 604 MMscf methane during ~2 years of operation. With horizontal borehole production, GIP in the Blue Creek seam decreased from an average of 1.52 MMscf to 1.23 MMscf per acre. It was also shown that effective gas flow capacity, which

*Tel.: +1 412 386 4008; fax: +1 412 386 6595. cok6@cdc.gov.

Disclaimer: The findings and conclusions in this paper are those of the authors and do not necessarily represent the views of the National Institute for Occupational Safety and Health (NIOSH). Mention of any company name, product, or software does not constitute endorsement by NIOSH.

Conversion Table (English to SI units)

| | | |
|---|---|---|
| 1 ft | = | 0.3048 m |
| 1 $ft^2$ | = | 22.957 × $10^{-6}$ acre |
| 1 MMscf | = | 28316 $m^3$ |
| 1 scfm | = | 0.0004719 $m^3/s$ |

Author Manuscript Author Manuscript Author Manuscript Author Manuscript

was independently modeled using vertical borehole data, affected horizontal borehole production. GIP and effective gas flow capacity of coal seam gas were also used to predict remaining gas potential for the Blue Creek seam.

### Keywords

History matching; Black Warrior basin; Coal mine methane; Degasification; Geostatistical simulation

## 1. Introduction

### 1.1. General issues and problem description

Ventilation of underground coal mines with an adequate amount of diluting airflow is important to prevent formation of explosive methane–air mixtures and to maintain methane concentrations in levels not exceeding 1% in an underground coal mine and 2% in bleeder systems. However, when gas contents of coal seams are high, or coal reservoir properties favor high methane emissions, ventilation alone may not be enough to keep methane levels within statutory limits. In that case, ventilation should be supported by other means of gas management, such as degasification using vertical or horizontal wells prior to coal mining (Karacan et al., 2011; Moore, 2012). A side benefit of degasification that is taken advantage of by most mine operators is to use or sell the produced gas as fuel.

During coal seam degasification using vertical boreholes, the geologic units termed as “coal groups” that contain multiple coal beds within a close distance to the mined seam are usually completed along the entire coal group. This practice allows for degasification of all coal seams of the group at the same time. However, since vertical boreholes, even with hydraulic fracturing, have limited reservoir contact, they usually need to produce for a long period of time to reduce gas-in-place (GIP) to safe levels that can be adequately handled by the ventilation system levels before mining starts. Therefore, in-seam horizontal boreholes are also drilled into the target coal bed from gateroad development entries usually 2–3 years in advance of the commencement of longwall operations. These boreholes are planned with various lengths and in different directions across the panel width in order to accelerate methane drainage from the coal and to decrease especially the face emissions during longwall mining (Karacan et al., 2007).

There are some uncertainties, however, with regards to evaluation of production efficiency of in-seam horizontal boreholes. The first uncertainty is related to the coal seam and the changes in its reservoir properties, especially at places where the boreholes are located. After degasification of the coal seam with vertical wellbores, initial reservoir properties that affect GIP and its deliverability to horizontal wells change over time. These reservoir properties include coal seam pressure, permeability, relative permeability, gas content, and water saturation, which control GIP and effective reservoir flow capacity, i.e. $k_{eff}h$, (Clarkson et al., 2011; Karacan, 2008, 2013; Saulsberry et al., 1996). These properties actually may be more important for in-seam wells than vertical wells due to their extensive reservoir contact. Therefore, past assessments of reservoir condition should be updated before planning in-seam degasification using horizontal wells. These values can be

Author Manuscript Author Manuscript Author Manuscript Author Manuscript

determined spatially, if there are enough vertical wells in the study area whose long-term production information can be analyzed by decline curve and via history matching methods (Karacan, 2013).

The second uncertainty is the appraisal of the exact location of in-seam wellbores and their individual production. Although geophysics coupled with drilling tools can give the exact position and direction of each well, they are attached together in the mine and only total production is monitored at the surface. Furthermore, if any well does not produce due to some unfavorable reservoir condition or borehole collapse, its location may not be diagnosed easily from the total production data without reservoir simulation and without assessing sensitivities to production (Keim et al., 2011). Even this may not be effective in that this practice will require spatially exact reservoir data. Therefore, it is not a misstatement to say that observed production from in-seam multilateral wells is from an "effective" horizontal wellbore positioned in an "effective" drainage area, whose size and boundaries are not well known but are related to the monitored production. Thus, a methodology to represent the "effective" horizontal wells and their "effective" drainage areas in coal seams can be highly valuable. This can be potentially achieved by production analyses, and by employing geostatistical simulations. Fig. 1 shows the flowchart of the methodology applied in this study and also the general structure of this paper.

### 1.2. Aims and methodology

This paper aims to address problems associated with the uncertainties discussed in previous paragraphs. It presents an integrated study and a multi-stage methodology including production data analyses and geostatistics for calculating GIP and its spatial distribution in a mining area in the Blue Creek seam, Alabama, after degasification with vertical and horizontal wellbores. In the course of the study, a method to represent "effective" horizontal wells in geostatistical degasification models with a comparison of results from sequential Gaussian simulation (SGSIM) and filter simulation (FILTERSIM), as well as using simulated maps of $k_{eff}h$ to interpret horizontal well production potentials, are discussed.

## 2. Description of the study site and the Blue Creek seam

### 2.1. Black Warrior basin and the study site

The degasification and mining site studied in this paper are located in the Black Warrior basin, where degasification activities started in 1971 in the Oak Grove field. These activities were planned as a 5-hole pattern drilled in Jefferson County with the involvement of the US Bureau of Mines. The objective was to reduce the emissions in an adjacent mine operated in the Mary Lee coal group.

The majority of the Black Warrior basin is located in the state of Alabama of the United States. The southeast margin of the Black Warrior basin has local anticlines and synclines due to strata upturned by folding. These are called Blue Creek anticline and syncline and are located northwest of a major thrust fault (Fig. 2). In addition to major structures shown in Fig. 2, the Black Warrior basin contains numerous northwest striking normal faults and joints, as shown in the study area in Fig. 2, which form horst and graben structures with displacements as much as 400 ft (McFall et al., 1986). These discontinuities are mostly due

Author Manuscript Author Manuscript Author Manuscript Author Manuscript

to formation of the sedimentary basin and also tectonic stress associated with the formation of the Appalachian front.

Tectonic maps prepared from various borehole logs and seismic reflection profiles indicate that the Pottsville formation in the southwestern edge of the Oak Grove field and the majority of the Brookwood field have normal faults (Groshong and Pashin, 2009). Thus, the impact of normal faults dissecting the Upper Pottsville formation may be present in gas and water production rates, as well as cumulative productions, of vertical wellbores of the study area.

Joints are more frequent with spacing between 6 and 10 inches, and oriented in N69W and N49E directions, respectively. As determined from outcrops, coal face cleats generally trend northeast (N62E) with spacing between 0.4 and 0.6 inches. Structural deformation in the general area has a significant effect on the performance of coalbed methane wells, mining emissions, and hydrodynamics (Pashin, 2007).

In addition to presence of natural cleats and joints in the coal seams, almost all vertical wells in the study area were fractured. Karacan (2013) predicted fracture half-lengths calculated at different well locations as long as 1100–1200 in the Mary Lee coal group. These hydraulic fractures generally dictate the directional permeability anisotropy. Gazonas et al. (1988) who conducted hydraulic fracturing tests and interpreted tiltmeter and geophysical data to estimate dip, direction, and growth of fractures around the boreholes observed that vertical fractures strike of N 78° E in the Mary Lee group with oblique orientations to face (N 61° E) and butt cleats.

The majority of the coal-bearing strata of economic value in the Black Warrior Basin are in the Pennsylvanian age Upper Pottsville formation. Coal bed gas is generally produced from depths shallower than 3000 ft (Pashin and Groshong, 1998). Initial degasification in the basin started with vertical boreholes, some of which were completed in 5–20 coal seams in the Pratt, Mary Lee and Black Creek coal groups (Pashin et al., 2010). Among these coal groups, the Mary Lee coal group is probably the most important due to mining of high-quality coal, as well as due to coal gas production activities.

The average depth of the Mary Lee coal group is between 1200 and 1950 ft in the study area (Fig. 3). Therefore, none of the coal seams of the Mary Lee group, which contains New Castle, Mary Lee, Blue Creek and Jagger coals (Fig. 3), outcrop within the study area. Within these coal seams, Mary Lee and especially Blue Creek seams are the main aquifers according to the resistivity log taken during drilling of the vertical degasification well 6141-C (Fig. 3).

The study area shown in Fig. 2 had 92 wells. However, 11 of them were completed in only the Pratt and Black Creek groups. The remaining 81 vertical boreholes had completions in the Mary Lee coal group, which contained Blue Creek coal. Therefore, the subsequent discussions and results will concentrate on these 81 vertical degasification wells.

Most of the vertical boreholes remained in production from the 1990s until 2010–2011 for about 6000 days. With the start of longwall mine planning and associated gateroad

Author Manuscript Author Manuscript Author Manuscript Author Manuscript

development in Blue Creek seam, horizontal in-seam boreholes were also drilled only into the Blue Creek coal starting in 2010. Vertical boreholes, on the other hand, were progressively terminated as the longwall operation commenced. It should be mentioned that structural faults, discussed earlier in this section and shown in the upcoming section, also had effects on mine planning and drilling of in-seam horizontal boreholes.

### 2.2. Coal and gas properties at the study area

The Mary Lee coal group covers an interval of about 150–250 ft (Fig. 3). In the study area, the thicknesses of the Blue Creek and Mary Lee seams vary between 2 and 9 ft, and 1 and 3 ft, respectively (Fig. 4). These two coal seams are separated by a parting layer, known as Middleman, whose thickness varies between 2 and 8 ft depending on the location (Figs. 3 and 4). The Mary Lee and Blue Creek seams merge into a single thick unit in the Southeastern part of the basin.

The Mary Lee and Blue Creek seams are valuable coal resources due to their quality and gas content. During coal mining, the Mary Lee and Blue Creek seams are usually mined together if the thickness of Middleman is small. Otherwise, the Blue Creek seam is the main mining target and is mined solo up to the Middleman layer.

The rank of these seams varies within the Black Warrior basin. In the study area, the Mary Lee/Blue Creek seam shows medium- to low-volatile bituminous coal characteristics with mean vitrinite reflectance (mean %Ro) values ranging between 1.2 and 1.4. Ultimate and proximate analyses results, on an “as received” basis, from a coal sample taken from the Blue Creek seam, as well as its petrographic composition, in the study area are shown in Table 1. Consistent with its rank, the Blue Creek seam also has a high gas adsorption potential confirmed with the Langmuir pressure ($P_L$) and Langmuir volume ($V_L$), also given in Table 1.

Quality of gas produced from degasification wells in the study area is generally high in methane, in excess of 98%. A gas sample taken from vertical degasification well 11090-C (shown in Fig. 2) showed ~98.5% $CH_4$, small amounts of $N_2$, $H_2$ and $CO_2$, and almost no higher hydrocarbons in the composition. The results of gas analysis are given in Table 2. However, it should be mentioned that this sample was taken from ~20-ft into the well from the wellhead, and also this borehole was completed at all three coal groups (Pratt, Mary Lee, and Black Creek). Thus, the gas composition given in Table 2 is a mixture of contributions from the coal seams of all coal groups. Nevertheless, the composition of gas from 11090-C and given in Table 2 was taken as representative of the gas produced in the study area, and 100% methane was used as the gas composition in all production data analyses.

Author Manuscript Author Manuscript Author Manuscript Author Manuscript

## 3. Reservoir properties, effective gas flow capacity and GIP of Blue Creek seam at the end of degasification using vertical wells

### 3.1. Post-degasification reservoir properties of the Blue Creek seam determined from history matching of vertical well productions

The original intent of coalbed methane production in the basin, when it started in the 1970s using vertical boreholes, was to decrease gas content of the coal seams to ensure safe mining. From a mining safety point of view, initial values of coal reservoir properties are important as they can control the potential amount of methane emissions into mines (Karacan, 2008). However, their change during or after degasification with vertical boreholes is also important, since the existing reservoir properties at the time of in-seam horizontal well drilling will dictate their productivity. In addition, computations using prevailing values enable estimating GIP and effective gas flow capacity of coal seams. Therefore, it is of the utmost importance to know the values of coal reservoir properties and their distributions in a mining and gas production site after vertical degasification and before horizontal well degasification starts.

Production analyses of all 81 vertical degasification boreholes completed in the Mary Lee coal group, along with the 11 wells having only Pratt and Black Creek completions, were conducted using history matching for both gas and water production. History matching computations and analyses were completed using Fekete's F.A.S.T. CBM™ software version 4.7 (Fekete Associates, 2012) independently for each well by honoring their completion intervals and properties of the seams in those coal groups. Fig. 5 shows history matching results for the 5603-C vertical well, as example, which was completed in two layers (Mary Lee and Black Creek coal groups). In this figure, solid lines show the simulated data for gas and water production from each coal group for which local reservoir properties could be determined. The details of the history matching process for vertical boreholes in this area and the primary considerations are given in Karacan (2013). In order to avoid a lengthy discussion by repeating details, readers are referred to that reference. Instead, in this paper the emphasis will be given to the results of history matching for present-day values of reservoir properties of the Mary Lee coal group and the Blue Creek seam. These values will be interpreted and discussed for determining remaining GIP and prevailing $k_{eff}h$ after degasification using vertical boreholes. These values will be further used as the initial condition for in-seam horizontal boreholes in 2010 and to interpret spatial efficiency of degasification after 3 years of horizontal well production.

For each of the 81 vertical wells of the study area, water and gas production were simulated starting from their first production date. Water and gas production history matching allowed estimation of the initial conditions of the coal seams in the 1980s at each well's spatial location, when the vertical boreholes in the study area first started production and to extract reservoir properties of the Mary Lee coal group for 2010. Time-dependent reservoir properties were determined during the history matching process by flagging the desired date, 2010 in this case, for data retrieval. This date is important as it has the values for coal reservoir properties, which allows for the computing of GIP and $k_{eff}h$ to estimate the remaining gas in the mining area before horizontal well production.

Author Manuscript Author Manuscript Author Manuscript Author Manuscript

It should be mentioned that history matching of well production enabled the prediction of permeability, relative permeability pressure, water saturation, and porosity for the entire Mary Lee coal group, which contains other seams, besides Blue Creek coal, in close proximity (Fig. 3). Therefore, reservoir properties predicted for the entire Mary Lee coal group should be assumed either as average (permeability, for example) or should be applied to individual coal seams within the group (i.e. pressure). Based on this condition, reservoir properties (i.e. pressure, water saturation, porosity) spatially predicted for the entire Mary Lee group at each wellbore location were considered also to apply to the Blue Creek seam at the same spatial locations. Blue Creek coal density and coal thickness were determined from each well's geophysical well logs. Gas content, on the other hand, was calculated using the pressure data at each location and the Langmuir parameters given in Table 1, assuming that Langmuir parameters apply all locations in the study area. This assumption, however, had to be implemented in the absence of relevant adsorption parameters at each well location.

Table 3 shows the results of the univariate statistical analyses for each of the coal reservoir properties in 2010 based on history matching analyses of 81 vertical wells. Since the data given in Table 3 belongs to a period when in-seam boreholes were just being drilled and put into production, they can be considered as the initial reservoir condition of the Blue Creek seam for production using in-seam horizontal boreholes. Fig. 6 shows the spatial distribution of these coal properties within the study area of Blue Creek seam.

### 3.2. Gas-in-place (GIP) and effective flow capacity ($k_{eff}h$) of Blue Creek coal prior to in-seam horizontal well production

Although individual reservoir parameters and their spatial distributions are very important for the appraisal of coal reservoir dynamics and fluid storage properties, evaluation of multiple parameters for computation of other physical properties usually provides better insights into availability of gas in the coal seam and for deliverability forecasting in degasification. In that respect, GIP and $k_{eff}h$ can be considered as two of the most important parameters. While GIP calculation estimates how much gas is available in a coal seam and how much gas may remain after degasification by considering time-lapse values of various reservoir parameters, GIP by itself may not guarantee high production from degasification wells unless there is sufficient permeability in the coal seam (Hamilton et al., 2012). In fact, high $k_{eff}h$, which is the product of absolute permeability, relative permeability, and reservoir thickness at any spatial well location, is essential for effective gas production. Therefore, the $k_{eff}h$ term appears in all well deliverability equations, whether the reservoir is coal or a conventional one, and is directly proportional to flow rate.

Volumetric GIP calculation is given in Saulsberry et al. (1996) and has been demonstrated by using available coal reservoir data and for various circumstances (Karacan and Goodman, 2012; Karacan et al., 2012; Karacan and Olea, in review). In this work, the 2010 values of the coal reservoir properties spatially shown in Fig. 4 allowed for computation of volumetric GIP in the Blue Creek seam for 2010 through the use of Eqs. (1) and (2). In the GC equation (Eq. (2)), P is the coal reservoir pressure prevailing in 2010 (psia), $V_L$ is the Langmuir volume (scf/ton), and $P_L$ is the Langmuir pressure (psia), respectively. Values of the Langmuir parameters measured at 86 °F are given in Table 1. Since Langmuir properties are

Author Manuscript Author Manuscript Author Manuscript Author Manuscript

reported on an “as received” basis, ash and moisture contents can be eliminated from Eq. (1) during calculations.

$$GIP_{2010}=Ah\left(\frac{43560(\phi_f\ (1-S_{wf}))_{2010}}{B_{g(2010)}}+1.359\,GC_{2010}\,\rho(1-f_a-f_m)\right) \quad (1)$$

$$GC_{2010}=\left(\frac{V_L\times P_{2010}}{P_L+P_{2010}}\right) \quad (2)$$

In these equations, GIP is the gas-in-place (Mscf); A is the area (acre); h is the thickness of coal; $\phi_f$ is the fracture porosity (fraction); $B_g$ is the gas formation volume factor (rcf/Mscf); $S_{wfi}$ is the interconnected fracture water saturation (fraction); GC is the gas content of the coal (scf/ton); ρ is the coal density (g/cc); $f_m$ is moisture content (fraction); $f_a$ is ash content (fraction); and both 43560 ($ft^2$/acre) and 1.359 [(Mscf)(ton)($cm^3$)/(ac-ft)(scf)(g)] are conversion factors. The reservoir parameters are for 2010, as indicated in the subscripts.

Gas flow capacity of a coal seam is a function of its effective permeability to gas and its thickness at a particular location. The latter is determined from density or gamma ray well logs. Effective permeability, on the other hand, is dictated by absolute permeability and relative permeability, both of which change spatially with time during the degasification process. Absolute permeability changes due to variations in porosity under the effect of matrix shrinkage in primary depletion, and relative permeability changes as a function of water saturation as water is produced from the coal reservoir. Therefore, effective gas flow capacity of the Blue Creek seam at spatial locations of the vertical wells can be determined using

$$(k_{eff}h)_{2010}=\left(k(\varphi_f)_{2010}k_r(S_w)_{2010}h\right) \quad (3)$$

In this equation, h is the coal thickness at the well location, $k(Ø_f)$ is the value of absolute permeability in 2010 that reflects changes due to coal-matrix shrinkage, and thus porosity during methane production from a particular well, $k_r(S_w)$ is the relative permeability as a function of water saturation determined using Corey functions at the same location.

Spatial $k_{eff}h$ and GIP maps shown in Fig. 7 are for 2010 and thus for the conditions before degasification using in-seam horizontal boreholes started. These maps show that $k_{eff}h$ ranged between 0.97 and 45.57 md.ft, and the highest values were in the north and northeast of the field. GIP, on the other hand, had minimum and maximum values of 0.32 MMscf and 3.69 MMscf per 0.92 acre (cell size), respectively. The highest GIP values were in the south of this field. Table 4 shows some statistical measures of $k_{eff}h$ and GIP values shown in Fig. 7.

Although $k_{eff}h$ and GIP are independent calculations, a careful examination of Fig. 7 suggests that $k_{eff}h$ and GIP are negatively cross-correlated at calculation points. In order to investigate spatial cross-correlation structure between these two variables, a cross-semivariogram map was prepared (Fig. 8). This map is a visual demonstration of cross-

Author Manuscript Author Manuscript Author Manuscript Author Manuscript

semivariance in every azimuth and can be used to find the major and minor principle axes of anisotropy. The center of the map is the center of cross-semivariogram in each direction and transects along each direction give the cross-semivariance, or cross-semivariogram, in those directions. The empty cells in the map are where there are no points to provide an average semivariance for a particular lag class and direction. In the cross-semivariance map, the direction of major anisotropy axis is along the longest spatial continuity corresponding to longest range, and thus to least average cross-semivariance. Similarly, the minor axis of anisotropy is along the shortest spatial continuity that corresponds to shortest range and highest average cross-semivariance. These two axes are located along NW–SE and NE–SW directions, respectively, with the azimuths shown in the map (Fig. 8).

The two cross-semivariograms shown in Fig. 8 in N 149° E and N 59° E directions show spatial continuity and negative cross-correlation between $k_{eff}h$ and GIP. Negative cross-correlation may make sense since as $k_{eff}h$ increases, the GIP calculated after degasification using vertical wells should decrease. However, more interesting are the directions of anisotropies and the ranges of these cross-semivariograms, which may be related to the structural features of the area and the directions of hydraulic fractures, joints and cleats. For instance, the cross-semivariogram in N 149° E direction lies closely along the major faults and with the direction of stress due to formation of regional anticlines and synclines. The range of this cross-semivariogram was determined as ~8100 ft and is close to the length of the blocks between normal faults. On the other hand, the cross-semivariogram in N 59° E direction is closely aligned with the directions of face cleats (N 61° E) and hydraulic fractures (N 78° E). The range of this cross-semivariogram was determined as ~5000 ft, which is close to the widths of the blocks between faults. Therefore, the negative cross correlation between $k_{eff}h$ and GIP has anisotropies and spatial continuities that are affected by the structure of the area.

## 4. In-seam horizontal boreholes in the Blue Creek seam prior to its mining and their production data analyses

### 4.1. Mine degasification area and the productions of in-seam horizontal boreholes

In-seam horizontal boreholes were drilled when a series of longwall panels were planned and gateroad development commenced in the study area. However, as mentioned in the site-description section, the area is dissected with vertical faults striking in the northeast direction. These faults also create major strata displacements.

Fig. 9 shows the three-dimensional view of the top of the Blue Creek seam with displacements due to faults and the outline of the planned mine area. Although each individual panel is not shown here, the widths of the panels were between 850 and 1000 ft with lengths between 15000 and 16000 ft. Longwall mining started in the area with the E1 panel, face advancing in the northeast direction, and mining was planned to continue to the E2–E6 panels (Fig. 9).

Since the main mining area in Blue Creek seam was in a horst structure isolated by two grabens on both sides, with downward displacements of ~150–170 ft in the west and 70–90 ft in the east, respectively (Fig. 9), it is clear that these faults are discontinuities for mining.

Author Manuscript Author Manuscript Author Manuscript Author Manuscript

In addition, these structures are discontinues for in-seam degasification of Blue Creek seam by compartmentalizing the coal gas reservoir and by affecting the continuity of any of the wells, if they are drilled crossing the fault lines. Therefore, in-seam degasification planning had to account for the presence and displacements due to these faults.

A total of 35 multi-lateral in-seam horizontal boreholes were drilled in the general mine area. One of these boreholes was outside of the main area of the E1–E6 panels, and three of them were not productive. Thus, there were 31 in-seam boreholes with gas production data. No water production was observed for any of the wells.

Fig. 10 shows the distribution of average daily gas rates (A) calculated based on 570 date events from all of these boreholes and the cumulative production from each well to date (B). The gas production rate distribution shown in Fig. 10-A had a mean of 40 Mscf/day with a standard deviation of 31.5. The maximum gas production rate was 170 Mscf/day. Cumulative production from 31 boreholes, on the other hand, had a mean value of 21.2 MMscf with a standard deviation of 10.9. The maximum (44.7 MMscf) and minimum (1.79 MMscf) cumulative gas productions were achieved by 16208-CH and 16209-CH, respectively (Fig. 10-B).

The locations of the in-seam boreholes were only designated with their geographic units, which define square areas in oil and gas fields. The centers of these geographic units with respect to mining boundaries are shown in Fig. 11. From this figure, one can see that the centers of all geographic units, and thus the boreholes, were located between the faults and within the marked rectangular area, where in-seam degasification took place in the Blue Creek coal. Fig. 11 also shows the locations of the vertical boreholes, which were discussed in the previous section and that produced until the start of mining.

It is known that in-seam boreholes of this area were mostly the multi-lateral type in-seam wells shown in Fig. 4-E in Karacan et al. (2007) drilled across the panel areas. However, no information related to their lengths and exact locations was provided to the Alabama Oil and Gas Board (AOGB) by the operator except for their geographic unit definitions. Furthermore, no information was available for the wells whether any laterals were unproductive or were producing more or less than the others. These facts call for the uncertainties that were described in the Introduction section and for the “effective” well concept, and we can conclude that the production values given in Fig. 10 are provided by those wells. Thus, the next step is to define the effective locations of these wells that will represent the physical locations for evaluation of the spatial degasification efficiency in the coal seam.

### 4.2. Production data analyses and revealing “effective” horizontal wells within the mine area

Depending on the data availability and the nature of the data, different approaches can be implemented for estimating drainage areas of horizontal wells. For instance, Olea et al. (2011b) used the known lengths of the wells and hydraulic fractures to estimate drainage areas in shale. In this work, production analyses of horizontal wellbores were performed using Fekete's F.A.S.T. CBM™ software version 4.7 (Fekete Associates, 2012). From

Author Manuscript Author Manuscript Author Manuscript Author Manuscript

production histories of 31 in-seam horizontal boreholes, only 21 were suitable for analyses. Others were either erratic or the durations were too short to be analyzed. Therefore, this analysis was performed for 21 boreholes.

Analytical horizontal well models were used for production modeling. The implementation of this model in the software is a single-phase flow reservoir. This is a suitable condition for a dry-coal reservoir, and also for the situation in this work where the coal reservoir has been produced by vertical boreholes for a long time prior to in-seam degasification and no additional water production of appreciable magnitude was observed during in-seam degasification. Also, the reservoir is a homogeneous medium, but in the sense that is not composite. Otherwise, the model permits three-dimensional anisotropy fluid flow properties.

The computation domain is formulated as a rectangular volume. However, the length and width of the reservoir, or the anticipated drainage area of the well, can be any positive value. Thus, depending on the wellbore production magnitude and production behavior, the dimensions and aspect ratio of the reservoir boundaries can vary. Moreover, the location of the horizontal well may be anywhere within the reservoir boundaries, provided that the wellbore does not overlap with any boundaries. Thus, it is possible to model the combined effects of horizontal wells and boundary flow by using Green's functions and the method of images (Dake, 1978) to calculate a full wellbore history from early-time to transition period into boundary-dominated flow in different geometrical configurations. In this solution, pseudo-time ($\Delta t$) and pseudo-pressure ($\Delta\Psi$) are used to accommodate changing gas compressibility and viscosity with reservoir pressure and to linearize gas flow equations.

The analytical model and its solution described in the previous paragraph can also be used to match production by error minimization. Therefore, effective drainage area and effective well length of a horizontal well, as well as its position within the reservoir boundaries can be estimated, given that the other reservoir properties are known or can be predicted for nearest locations and within the anticipated reservoir volume as the initial reservoir properties. In this work, the values of the Blue Creek coal's reservoir data given in Fig. 6, deemed representative at the closest locations to the horizontal wells, were used as the initial properties for in-seam degasification modeling.

Fig. 12 shows a set of results for modeling production of 15779-CH. Figs. 12-C and D show simulated cumulative production versus production rate, and time versus gas production rate, respectively, and their comparison with field data. Fig. 12-D also shows that the average reservoir pressure declined from ~130 psia from its 2010 value at that location to below 110 psia as a result of production using in-seam degasification within 1.5 years. Fig. 12-B, on the hand, shows a plot of type curves for pseudo pressure ($\Delta\Psi$) with respect to pseudo-time ($\Delta t$), and its derivative driven from this match. Type-curves are basically the solutions representing the particular theoretical model. These type curve solutions can be processed further with a set of general type curves to devise more data related to the reservoir. They also indicate the flow regimes that the boreholes are experiencing. For instance, early times in Fig. 12-B is a signature of vertical radial flow, whereas later times show linear flow to the well.

Author Manuscript Author Manuscript Author Manuscript Author Manuscript

The information that is of particular interest for this paper is the size of the drainage area and the effective wellbore length and its position with respect to the boundaries. This information predicted for 15779-CH is shown in Fig. 12-A. This figure shows that the effective 15779-CH is approximately 1800 ft in length and is located off-centered in the estimated drainage area of ~133 acres. Similar modeling and analyses described in the previous paragraph were conducted for each of the 21 in-seam wells analyzed.

The next step was to locate the effective horizontal wells with respect to the center of the geographical unit locations in the general area shown in Fig. 11. This was accomplished by coinciding the geometric center of the drainage areas (e.g. Fig. 12-A) with the spatial location of the center of the geographic units that they belonged to (Fig. 11). Once these two points, one arbitrary and the other defined spatially, were matched in real coordinates, effective wells were projected to their corresponding spatial locations based on their lengths and their off-sets from center points. Positioning effective wells enabled defining boundaries of the total drainage area, which was determined to be approximately 2050 acres. This area included 31 wells that collectively produced a cumulative gas of ~650 MMscf. Spatial locations of effective wells in real coordinates and the boundary of the effective drainage area are shown in Fig. 13.

As can be noted from Fig. 13, the process outlined above results in apparent clustering of the effective well locations into several E–W bands associated with the geographical units. Although this direction and clustering is the result of the effort of developing a methodology defining the wells, for which exact places and lengths are not known, and also the result of the effort of placing effective horizontal wells in spatial coordinates, it is not too far from reality either; in reality multilateral in-seam boreholes in this area are drilled in cross-panel directions. However, considering that some of the laterals may not be as productive as others (even unproductive), the effective direction of the entire multilateral may not be the exact drilling direction and may very well be aligned in the general E–W direction. Since, as shown later, the production analysis is based on simulating specific productions, this approach is not expected to adversely affect the results.

The results of the analyses presented in this section for effective horizontal wells are shown in Table 5. This table includes both the wells that could be modeled and also the ones that could not, but were in the boundaries of the effective degasification area shown in Fig. 13 and produced gas. The data in the table gives cumulative production from each well and specific production calculated using estimated effective borehole lengths and drainage areas. Further, the latter made it possible to calculate cumulative production per 0.92 acre, which was equivalent to a cell size in the geostatistical models. This production estimated for per-cell of the drainage area for each well was collocated with borehole grids and simulated using the geostatistical modeling approach proposed in the upcoming sections of this paper.

## 5. Geostatistical modeling of in-seam methane drainage and its efficiency

### 5.1. Sequential Gaussian simulation (SGSIM) and filter simulation (FILTERSIM) paradigms

Geostatistical analyses and modeling techniques have been widely used for coal resource evaluation and mining (e.g. Heriawan and Koike, 2008; Olea et al., 2011a; Karacan et al.,

Author Manuscript Author Manuscript Author Manuscript Author Manuscript

2012; Karacan and Goodman, 2012; Olea and Luppens, 2012; Karacan and Olea, in review). Most recently, a special issue of *International Journal of Coal Geology* compiled papers by the leading experts working in coal and geostatistics on applications of geostatistical techniques to coal science, coal geology and related sciences (Olea, 2013). These papers demonstrated the current application of geostatistics to coal-related studies, on spatially correlated data, mostly by 2-point statistics using variogram-based techniques such as kriging, and stochastic simulation methods. An introductory paper by Srivastava (2013) on the same issue reviewed details of various variogram-based geostatistical techniques used in these papers, discussing advantages and disadvantages. Readers are referred to that paper, as well as others (Deutsch and Journel (1998), Remy et al. (2009), Olea (2009)) for the theory and in-depth review of various geostatistical techniques.

Geostatistics can be used to account for a wide range of data types of varying resolution, quality, and uncertainty at different scales. It has been observed that complex patterns, discontinuities, and curvilinear shapes are poorly reproduced by variogram-based 2-point statistics (Zhang, 2008). Multiple-point statistics (mps) was proposed by Journel (1992) to overcome these problems and extended by the use of a training image (TI) by Guardiano and Srivastava (1992). The mps concept was later made practical with the SNESIM (Strebelle, 2000) algorithm, which was able to model only categorical variables. In order to resolve various issues of previous mps algorithms, filter-based simulation, FILTERSIM, was proposed by Zhang et al. (2006). FILTERSIM is also a pattern-based approach and simulates patterns conditional to local data. FILTERSIM is capable of simulating strong anisotropies and discontinuities (such as displacement faults) that cannot be represented by semivariograms and in simulation of continuous variables.

In FILTERSIM, the sequential simulation paradigm (Deutsch and Journel, 1998) was extended to extract a conditioning data while applying a search template along a random path in the simulation grid. During this process, using the training pattern prototype closest to that data based on a distance calculation method, the filter score distance is found. Then, a pattern is stochastically picked from the prototype class closest to the conditioning data and pasted on the simulation grid. The simulation proceeds sequentially from the coarser grid towards the finer one based on patch dimensions. Thus, during simulations, the inner part of this patch data is kept as hard data in the simulation grid and is not visited again during the same run, while the coarse grid is re-visited until all multi-grids are simulated (Remy et al., 2009).

SGSIM and FILTERSIM and their SGeMS implementations are discussed in detail in Wu et al. (2008a,b) and in Remy et al. (2009). In this work, these two techniques were used to simulate cumulative gas production from effective horizontal wells' total drainage area in the Blue Creek seam for comparison purposes. FILTERSIM was further used for the same area in GIP and $k_{eff}h$ modeling to integrate with in-seam horizontal well production maps.

### 5.2. Geostatistical modeling of cumulative in-seam gas production of effective wells from the total drainage area

Geostatistical simulation differs from kriging in its ability to reproduce global features and statistics where reproduction of patterns of spatial continuity is maintained. Although there

Author Manuscript Author Manuscript Author Manuscript Author Manuscript

are no clear rules to exclude either kriging or simulation from a geostatistical analysis, except for some considerations stated above where kriging equations fail, in this work simulations are preferred over kriging for modeling of spatial continuity and for stochastic assessment of the attributes. Therefore, SGSIM and FILTERSIM were used as the preferred techniques to model productions from in-seam wells.

SGSIM is a 2-point statistical technique that requires a variogram, where FILTERSIM is a multi-point statistical technique that requires a training image (TI) where the data patterns are conditioned to local data. In either case, spatially representative data are required. Thus, as the first step, the 2050-acre total drainage area estimated from horizontal well production analyses (Fig. 13) was defined and gridded with a total of 2222 simulation cells, each of which was 200 ft in x- and y-directions, respectively, to give an individual cell area of 0.92 acres.

Creating a computation grid was followed by defining the grid addresses of effective wells, shown in Fig. 13, in the model and by locating them onto the computation grid according to their effective lengths. The data associated with each wellbore grid was the average cumulative gas production estimated per 0.92 acres of each well's drainage area. These data are given in the last column of Table 6. These data, for each effective in-seam well, were collocated with wellbore cells. One may question why the data were only collocated with the wellbore cells. The justification for this decision was that the only locations for which these values could be known, within the accuracy of the analyses, were wellbore grids, and those are where the models could be conditioned to. Other locations are more likely susceptible to stochastic processes and the effects of the values nearby while generating cumulative production maps. The collocated spatial cumulative production data, as a classed map, within the model grid is shown in Fig. 14-A. This data was used to build a semivariogram using normal-scored values. The omni-directional semivariogram that was used in SGSIM is shown in Fig. 15.

Unlike SGSIM, FILTERSIM aims to capture patterns or structures from training images (TI) and condition them to local data in pattern classification and simulation. Although TI can be conceptual and does not have to be precise in the FILTERSIM application, it is suggested that realistic training images are crucial for the success of the simulation (Olea, 2009). Therefore, special attention was given to produce statistically representative TI for the spatial data shown in Fig. 14-A. For this purpose, a TI grid of the same dimensions and grid counts as the simulation grid was created and the grids were assigned values using first order Voronoi decomposition (nearest-neighbor) approach. The TI created using the data shown in Fig. 14-A is given in Fig. 14-B. The training image was examined by comparing its statistics with those of actual data using basics statistics and Q-Q plots, which indicated statistical similarity and representativeness of TI to the actual data (Karacan and Olea, in review).

In FILTERSIM, patterns are captured from TIs by sliding a set of filters, which are basically weights associated with a search template, and associating similar patterns with similar vector scores (Wu et al., 2008a). In this work, K-means clustering was used, in which the optimal centroid of each cluster is associated with the training patterns based on the distance, score-based distance, between patterns, and cluster centroids (Wu et al., 2008a,b).

Author Manuscript Author Manuscript Author Manuscript Author Manuscript

The simulations were conditioned to hard data only and have not been forced to match the TI histogram. However, simulation parameters including the number of clusters, clustering method, search template, and patch dimensions can affect the results. Therefore, these parameters were optimized as also demonstrated in Karacan and Olea (in review).

Sequential simulations create a single realization for each stochastic draw. Each realization can be seen as a numerical model of possible distribution of the simulated property in space. In this work, 100 realizations using both SGSIM and FILTERSIM were generated for cumulative gas production of effective horizontal boreholes from the drainage area. This set of simulations was used for statistical analyses and for evaluation of uncertainty. However, for presenting simulation results as maps, E-type maps, which can be viewed as the spatially averaged realization of all simulations, were used.

Fig. 16 shows E-type maps of cumulative gas production from the drainage area by effective horizontal wells. The E-type of SGSIM was obtained using the data in Fig. 14-A and the semivariogram shown in Fig. 15. The E-type of FILTERSIM results, on the other hand, was obtained using the TI shown in Fig. 14-B. These two maps show that the results obtained using two different simulations are similar in value magnitudes and the spatial distributions of values. It seems, however, that FILTERSIM represents the continuity of data at well locations a little better in this case and preserves the patterns more realistically. However, this may partly be due to using an isotrophic semivariogram in SGSIM.

A cell-value-based comparison of statistical measures of each realization obtained from SGSIM and FILTERSIM is given in Fig. 17. This figure shows three quartiles (Q25, Q50 (median), and Q75), mean, and standard deviation based on 2222 cell values. The data shows most values are close to each other, including standard deviations, between SGSIM and FILTERSIM, with the exception of the Q25 values which are consistently higher in FILTERSIM realizations and are within the standard deviation range. Nevertheless, the lower end of the cell-based cumulative production range of values does not affect the mean, Q50, and the standard deviation noticeably. The same statistical measures for the E-type maps are given in Table 6.

Fig. 18 shows histograms of cumulative gas production calculated for the 2050-acre drainage area from all 100 realizations of each simulation method. These data show that the cumulative gas production obtained using SGSIM varied between a minimum ~476 MMscf and a maximum ~664 MMscf. The mean value of 100 SGSIM realizations was ~559 MMscf. The same measures for FILTERSIM realizations were ~528 MMscf, ~686 MMscf, and ~604 MMscf, for minimum, maximum, and mean, respectively. The 5%, 50%, and 95% quantiles (Q5, Q50, and Q95) determined by ranking the cumulative gas production values obtained from all realizations, and the value of E-type are given in Table 7. Basically, quantiles indicate the probability of cumulative gas productions calculated using simulations being lower (or larger) than the associated value. For instance, using FILTERSIM, a Q50 of ~600 MMscf indicates that the true value can be lower than this value with a 50% probability. Thus, lower quantile values (Q5) indicate the lower limits whereas the highest quantile (Q95) indicate the highest limit in which the true value can be located. Thus, these values give a sense of uncertainty range for the results of simulations.

Author Manuscript Author Manuscript Author Manuscript Author Manuscript

The quantile values given in Table 7 show that the simulated cumulative gas productions are within 40 MMscf and 50 MMscf, when SGSIM and FILTERSIM results are compared. This translates to an average cell-based difference between 0.0180 MMscf and 0.0225 MMscf between these two simulation methods. Furthermore, in Table 7, the quantile values and the values of E-type are compared with the actual cumulative production enclosed by the effective drainage area. These values show that Q95 values of simulations especially that of FILTERSIM are very close to the measured cumulative production from wells within the drainage area. At this point, it is worth mentioning that the observed cumulative gas production (656.9 MMscf) lies in the upper tail (> Q95) for the distribution resulting from SGSIM, and just below Q95 for the FILTERSIM results, rather than close to Q50. This may be due to the fact that effective well lengths and drainage areas are from production analysis, from which collocated specific productions were used for simulations. Thus, any small discrepancies in lengths and areas from that independent analysis may result in shifting the distribution of simulated quantities. Nevertheless, simulation results can be considered close to observed cumulative production, which suggests that applied methodology including the production data analyses for horizontal wells to determine effective boreholes and the drainage areas for in-seam degasification provides results that may be considered acceptable.

In calculation of remaining gas in the Blue Creek seam due in-seam degasification and in computation of $k_{eff}h$ in the drainage area, FILTERSIM was used in lieu of SGSIM as the simulation technique. This choice was made not only in the light of results and discussions so far, but also due to the anisotropies that were difficult to capture with semivariograms.

### 5.3. Computation of remaining gas in place (R-GIP) in the Blue Creek seam as the result of in-seam degasification before mining

Computation of remaining gas-in-place (R-GIP) due to in-seam degasification requires the knowledge of initial GIP after degasification with vertical wells and cumulative production (CP) by horizontal wells. Initial GIP at vertical borehole locations was calculated as described in Section 3.2 using coal reservoir properties of 2010 in Eqs. (1) and (2). These data at vertical borehole locations are shown in Fig. 7. In order to maintain consistency with the CP computations, FILTERSIM was used to simulate these GIP data through a TI, which was created and tested as described in the previous section.

One hundred GIP realizations belonging to the completion of vertical borehole degasification were generated and the model area corresponding to the effective drainage area of the horizontal wells was extracted from each realization. These realizations constituted a set of 100 GIP realizations for the effective drainage area in the Blue Creek seam prior to the start of in-seam degasification. In order to determine R-GIP realizations of the same area and to assess its uncertainty, the CP realizations generated during the step discussed in the previous section were subtracted from each of the GIP realizations. This set of 100 R-GIP realizations was used for post-simulation analyses and for quantification of uncertainty for the gas amount that is left in the Blue Creek seam prior to mining.

The GIP and R-GIP realizations were ranked with their cumulative values to determine the realizations that corresponded to Q5, Q50, and Q95. These realizations were used to

Author Manuscript Author Manuscript Author Manuscript Author Manuscript

compare the values and to quantify the uncertainty in GIP and R-GIP. Table 8 shows a comparison of Q50 realizations with the statistical merits of 2222 cell values. The data shows that minimum GIP of the Q50 realization was 0.492 MMscf per 0.92 acre before in-seam degasification, which decreased to 0.086 MMscf after horizontal well production. Similarly, maximum GIP cell value was 3.689, which decreased to 2.575 MMscf after degasification using in-seam boreholes. The difference represents more than 1 MMscf decrease in a 0.92 acre area in 1.5–2 years of horizontal well production. Similar decreases in GIP are observed in quartiles and in the mean of the cell value distribution.

Fig. 19 shows the E-type maps of GIP and R-GIP based on 100 realizations. These maps spatially show the effect of in-seam degasification in reducing GIP in the drainage area of horizontal wells. The data shows that a large mine area within the Blue Creek seam was degasified with GIP-per-cell values decreasing between 0.25 and 1.0 MMscf, depending on the location. It is also noticeable that the western edge of the drainage area where in-seam boreholes were more frequent were degasified more effectively, showing the importance of drilling horizontal boreholes as frequently as practical and economically feasible in gassy coal seams.

The relative frequency histograms of cumulative GIP and R-GIP values of individual realizations are shown in Fig. 20. These histograms show that there is a clear shift of R-GIP from the initial GIP as a result of in-seam degasification. The mean amount of methane in the effective drainage area decreased from ~3185 MMscf to 2567 MMscf due to in-seam degasification. This decrease is consistent with the cumulative production computed with the effective well concept and with measured amount of gas from in-seam wells.

In order to quantify the spread of data distribution (Fig. 20) and to quantify the uncertainty inherent to computations, Q5, Q50, and Q95, as well as E-type, values of GIP and R-GIP were determined and are given in Table 9. This table shows that GIP at Q95 is ~3400 MMscf, whereas the Q5 value is ~3000. Therefore, it is not likely that the GIP before in-seam degasification will be less than 3000 MMscf in this area. However, the maximum expected value can be as much as 3400 MMscf with a median (Q50) value of 3190 MMscf. After in-seam degasification reported in this work, R-GIP can be as much as ~2800 MMscf, but not less than ~2400 MMscf. The median of the expected values for R-GIP is ~2550 MMscf. These values, in combination with the cell data given in Table 8, show that ventilation of the mine after in-seam degasification should be planned for ~1.1 MMscf methane per 0.92 acre (median), or for ~2550 MMscf (Q50) methane from the 2050 acre area of Blue Creek seam. Of course, these values are only for Blue Creek seam, excluding potential roof and floor emissions from other coals (Karacan and Olea, in review), which are not affected by in-seam degasification.

### 5.4. Relation of Blue Creek coal's reservoir f;ow capacity ($k_{eff}h$) to cumulative production (CP) and to R-GIP

Effective flow capacity ($k_{eff}h$) of any reservoir is very important for deliverability of fluids to wells. Coal seam reservoirs are no exception. A coal seam may have high gas content or high GIP; however, if there is not sufficient flow capacity of coal seam for gas, then it will be difficult to remove gas from the coal seam using vertical or horizontal wells. Therefore,

Author Manuscript Author Manuscript Author Manuscript Author Manuscript

cumulative production (CP) and R-GIP in the effective drainage area should be related to $k_{eff}h$.

Spatial distribution of $k_{eff}h$ after degasification using vertical wells in the study area was simulated using FILTERSIM and the data given in Fig. 7. The values within the effective drainage area are within a range of 3 and 20, with a median value of 11.84 md.ft, and where the highest values are located close to the middle of the drainage area. The E-type map of $k_{eff}h$ and a probability map of values higher than the median for $k_{eff}h$ and smaller than median of R-GIP (1.101 MMscf) are shown in Fig. 21. Thus, in-seam wells located in high-$k_{eff}h$ regions, if any, have a better chance of producing more CP or more gas per length of the wellbore, and also leaving less R-GIP in the coal when the mining starts. A comparison of the R-GIP map given in Fig. 19 with the maps shown in Fig. 21 indicates that this, in fact, is the case, and that lesser R-GIP areas as a result of in-seam degasification are closely located with where the high-$k_{eff}h$ areas are. This also suggests that these two events simultaneously occur with higher probability at locations that have higher $k_{eff}h$ values compared to rest of the coal reservoir in the drainage area. It should also be noted that the GIP, CP (or R-GIP), and $k_{eff}h$ are independent computations. Therefore, having meaningful results and spatial distributions that conform to expectations is an indication of the general merit of the approach proposed in this work.

## 6. Summary and conclusions

This paper presented an integrated methodology combining production data analyses of vertical degasification and horizontal in-seam wells, and geostatistical simulation algorithms to estimate R-GIP in a coal seam prior to mining. The proposed methodology was applied to Blue Creek seam, Alabama.

The first part of the methodology included production data analyses of vertical wells, which had been producing since the 1980s, to determine coal reservoir properties at a certain date as the result of gas and water production. This date was the beginning of 2010, when mine development roadways for longwall mining began development and degasification using vertical wellbores practically ended. Using the reservoir data at this time, gas-in-place and effective flow capacity ($k_{eff}h$) as of the end of vertical degasification could be calculated at spatial locations.

With the development of mine entries, in-seam horizontal boreholes were drilled into the Blue Creek seam for further degasification for about 2 years prior to start of longwall mining. Thus, the second stage of the method included production data analyses of in-seam wells to determine effective horizontal well, cumulative production per grid and effective drainage area. These would represent the gas production from the seam at the start of longwall mining and quantify the additionally degasified area.

The third step was stochastic geostatistical modeling, where cumulative gas production could be estimated from the effective drainage area and its spatial properties. Sequential Gaussian simulation and filter-simulation were used. These two techniques gave close results to the actual production amount of 650 MMscf from the coal using in-seam holes. Spatial GIP data at the end of the vertical degasification period was also modeled and used

Author Manuscript Author Manuscript Author Manuscript Author Manuscript

for calculating remaining gas in the coal seam prior to the start of longwall development mining. In addition, $k_{eff}h$ of the same period was also modeled to relate it to in-seam productivity.

General conclusions of the study are that the methodology is intensive but produces area-wide realistic results to degasification of coal seams since it combines both reservoir engineering techniques and geostatistics. The data showed that using in-seam wells, the median GIP per 0.92 acre of the area (cell size) decreased from ~1.3 MMscf to ~1.1 MMscf. The cumulative GIP reduction in the drainage area was about 600 MMscf, which resulted in a remaining GIP value of 2500 MMscf.

It has been observed, as a result of independent computations, that gas production using in-seam wells was related to the reservoir flow capacity of the coal seam at the end of degasification using vertical wells. The $k_{eff}h$ within the studied drainage area was between 3 and 20 md.ft, with a median of 11.84. Comparison of CP and R-GIP, and $k_{eff}h$ showed that higher fiow capacity areas were associated with higher cumulative production and less remaining methane in the coal. This finding should be considered when planning in-seam degasification prior to mining and to plan more in-seam drilling to degasify problem areas more effectively.

Overall, the integrated methodology presented here will help in evaluating various stages of degasification and the state of the coal seam prior to mining, and will help to reduce uncertainties associated with in-seam degasification discussed in the Introduction section. This approach will be helpful to gas control and ventilation engineers and thus is an improvement to ensure safe mining.

## Supplementary Material

Refer to Web version on PubMed Central for supplementary material.

## Acknowledgments

Dr. Jack Pashin and Richard Carroll of the Alabama Geological Survey are appreciated for their help in providing data for this work. Also, two anonymous reviewers appointed by the journal are thanked for their comments that helped improving the quality of the earlier version of this paper.

## References

Clarkson CR, Rahmanian M, Kantzas A, Morad K. Relative permeability of CBM reservoirs: controls on curve shape. International Journal of Coal Geology. 2011; 88:204–217.

Dake, LP. Fundamentals of Reservoir Engineering. Elsevier; Amsterdam: 1978. p. 443

Deutsch, CV.; Journel, AG. GSLIB Geostatistical Software Library and User's Guide. 2. Oxford University Press; New York, NY: 1998. p. 369

Fekete Associates. FAST CBM (2012). Calgary, Alberta, Canada: 2012.

Gazonas, GA.; Wright, CA.; Wood, MD. Tiltmeter mapping and monitoring of hydraulic fracture propagation in coal: a case study in the Warrior Basin, Alabama. In: Fassett, JE., editor. Geology and Coalbed Methane Resources of the Northern San Juan Basin, Colorado and New Mexico. Rocky Mountain Association of Geologists; Denver, Colorado: 1988.

Groshong RH, Pashin JC. Structural controls on fractured coal reservoirs in the southern Appalachian Black Warrior foreland basin. Journal of Structural Geology. 2009; 31:874–886.

Author Manuscript Author Manuscript Author Manuscript Author Manuscript

Guardiano, F.; Srivastava, RM. Multivariate geostatistics: beyond bivariate moments. In: Soares, A., editor. Proceedings of the 4th International Geostatistics Congress. Vol. 1. Kluwer Academic Publications; Dordrecht, Netherlands: 1992.

Hamilton SK, Esterle JS, Golding SD. Geological interpretation of gas content trends, Walloon Subgroup, eastern Surat Basin, Queensland, Australia. International Journal of Coal Geology. 2012; 101:21–35.

Heriawan MN, Koike L. Identifying spatial heterogeneity of coal resource quality in a multilayer coal deposit by multivariate geostatistics. International Journal of Coal Geology. 2008; 73:307–330.

Journel, AG. Geostatistics: roadblocks and challenges. In: Soares, A., editor. Proceedings of the 4th International Geostatistics Congress. Vol. 1. Kluwer Academic Publications; Dordrecht, Netherlands: 1992.

Karacan CÖ. Evaluation of relative importance of coalbed methane reservoir parameters for prediction of methane inflow rates during mining of longwall development entries. Computers and Geosciences. 2008; 34:1093–1114.

Karacan CÖ. Production history matching to determine reservoir properties of important coal groups in Upper Pottsville formation, Brookwood and Oak Grove fields, Black Warrior Basin, Alabama. Journal of Natural Gas Science and Engineering. 2013; 10:51–67. [PubMed: 26191096]

Karacan CÖ, Goodman GVR. Analyses of geological and hydrodynamic controls on methane emissions experienced in a Lower Kittanning coal mine. International Journal of Coal Geology. 2012; 98:110–127.

Karacan CÖ, Olea RA. Time-lapse analysis of methane quantity in the Mary Lee group of coal seams using filter-based multiple-point geostatistical simulation. Mathematical Geosciences. in review.

Karacan CÖ, Diamond WP, Schatzel SJ. Numerical analysis of the influence of in-seam horizontal methane drainage boreholes on longwall face emission rates. International Journal of Coal Geology. 2007; 72:15–32.

Karacan CÖ, Ruiz FA, Cotè M, Phipps S. Coal mine methane: a review of capture and utilization practices with benefits to mining safety and to greenhouse gas reduction. International Journal of Coal Geology. 2011; 86:121–156.

Karacan CÖ, Olea RA, Goodman GVR. Geostatistical modeling of gas emissions zone and its in-place gas content for Pittsburgh seam mines using sequential Gaussian simulation. International Journal of Coal Geology. 2012; 90–91:50–71.

Keim SA, Luxbacher KD, Karmis M. A numerical study on optimization of multilateral horizontal wellbore patterns for coalbed methane production in Southern Shanxi Province, China. International Journal of Coal Geology. 2011; 86:306–317.

McFall KS, Wicks DE, Kuuskra VA. A geologic assessment of natural gas from coal seams in the Warrior Basin of Alabama. GRI Topical Report. 1986:86–0272. 80.

Moore TA. Coalbed methane: A review. 2012. International Journal of Coal Geology. 2012; 101:36–81.

Olea RA. A Practical Primer on Geostatistics. US Department of the Interior: US Geological Survey, Open-File Report 2009–1103. 2009:346.

Olea, RA. Special issue on geostatistical and spatiotemporal modeling of coal resources. International Journal of Coal Geology. 2013. http://dx.doi.org/10.1016/j.coal.2013.01.010

Olea RA, Luppens JA. Sequential simulation approach to modeling of multi-seam coal deposits with an application to the assessment of a Louisiana lignite. Natural Resources Research. 2012; 21:443–459.

Olea RA, Luppens JA, Tewalt SJ. Methodology for quantifying uncertainty in coal assessments with an application to a Texas lignite deposit. International Journal of Coal Geology. 2011a; 85:78–90.

Olea RA, Houseknecht DW, Garrity CP, Cook TA. Formulation of a correlated variables methodology for assessment of continuous gas resources with application to the Woodford play, Arkoma Basin, eastern Oklahoma. Boletín Geológico y Minero, Madrid. 2011b; 122(4):483–496.

Pashin JC. Hydrodynamics of coalbed methane reservoirs in the Black Warrior Basin: Key to understanding reservoir performance and environmental issues. Applied Geochemistry. 2007; 22:2257–2272.

Author Manuscript Author Manuscript Author Manuscript Author Manuscript

Pashin JC, Groshong RH. Structural control of coalbed methane production in Alabama. International Journal of Coal Geology. 1998; 38:89–113.

Pashin, JC.; Carroll, RE.; McIntyre, MR.; Grace, RLB. Geology of unconventional gas plays in the southern Appalachian thrust belt. Guidebook for field trip 7, AAPG Annual Conference and Exposition; April 14–16; New Orleans, LA.. 2010.

Remy, N.; Boucher, A.; Wu, J. Applied Geostatistics with SGeMS, A User's Guide. Cambridge University Press; Cambridge, United Kingdom: 2009. p. 264

Saulsberry, JL.; Schafer, PS.; Schraufnagel, RA., editors. Gas Research Institute Report GRI-94/0397. Illinois, Chicago: 1996. A Guide to Coalbed Methane Reservoir Engineering.

Srivastava, M. Geostatistics: a toolkit for data analysis, spatial prediction and risk management in the coal industry. International Journal of Coal Geology. 2013. http://dx.doi.org/10.1016/j.coal.2013.01.011

Strebelle, S. PhD Thesis. Stanford University; Stanford, CA: 2000. Sequential simulation drawing structures from training images; p. 187

Wu J, Boucher A, Zhang T. A SGeMS code for pattern simulation of continuous and categorical variables: FILTERSIM. Computers and Geosciences. 2008a; 34:1863–1876.

Wu J, Zhang T, Journel A. Fast FILTERSIM simulation with score-based distance. Mathematical Geosciences. 2008b; 40:773–788.

Zhang T. Incorporating geological conceptual models and interpretations into reservoir modeling using multiple-point geostatistics. Earth Science Frontiers. 2008; 15:26–35.

Zhang T, Switzer P, Journel AG. Filter-based classification of training image patterns for spatial simulation. Mathematical Geology. 2006; 38:63–80.

## Appendix A. Supplementary data

Supplementary data associated with this article can be found in the online version, at http://dx.doi.org/10.1016/j.coal.2013.02.011. These data include Google maps of the most important areas described in this article.

Author Manuscript Author Manuscript Author Manuscript Author Manuscript

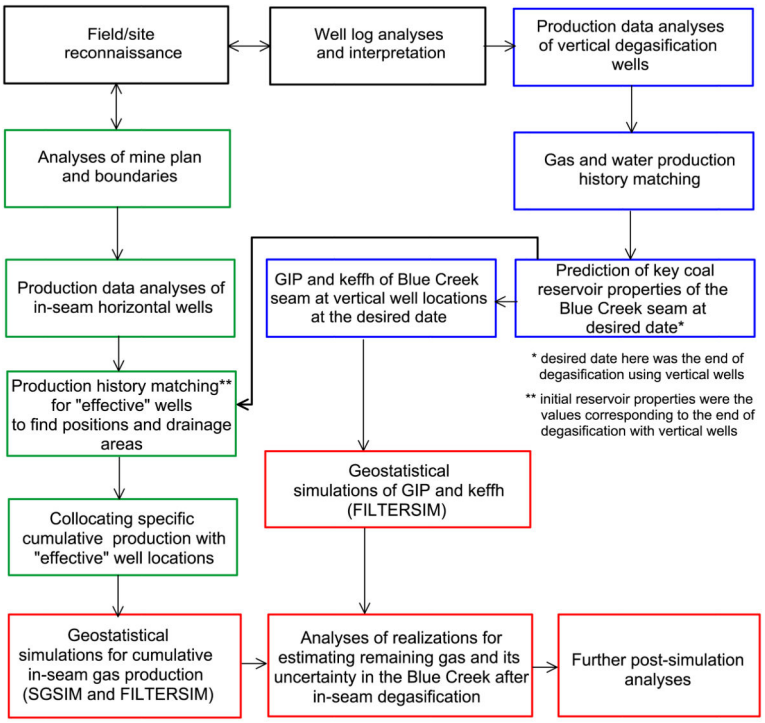


**Fig. 1.**

Flowchart of the general methodology applied in this study. Different box colors refer to different phases of the study.

Author Manuscript Author Manuscript Author Manuscript Author Manuscript

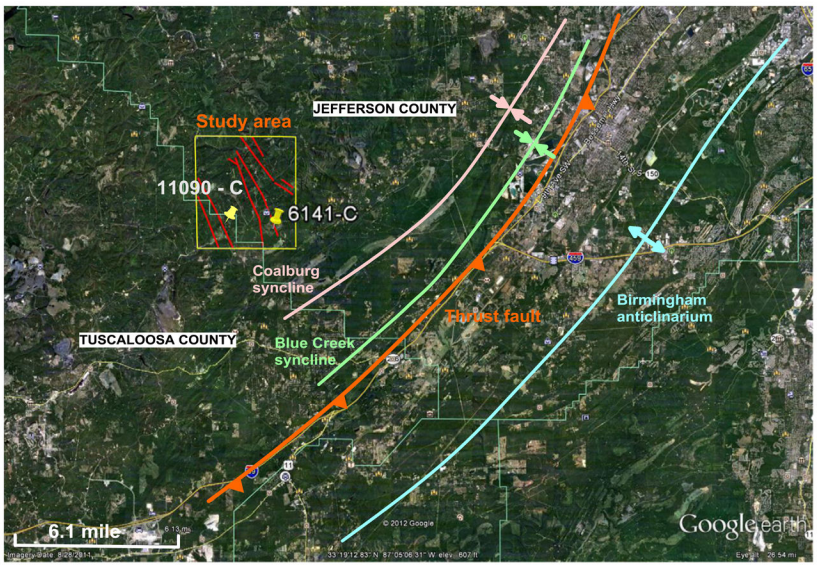


**Fig. 2.**

Major anticlines and synclines along the upturned margin of the Black Warrior basin. The aerial photograph also shows the study area of this paper with major displacement faults within. The location markers show the wells from which gas samples (11090-C) and the geophysical logs (6141-C) are presented.

Author Manuscript Author Manuscript Author Manuscript Author Manuscript

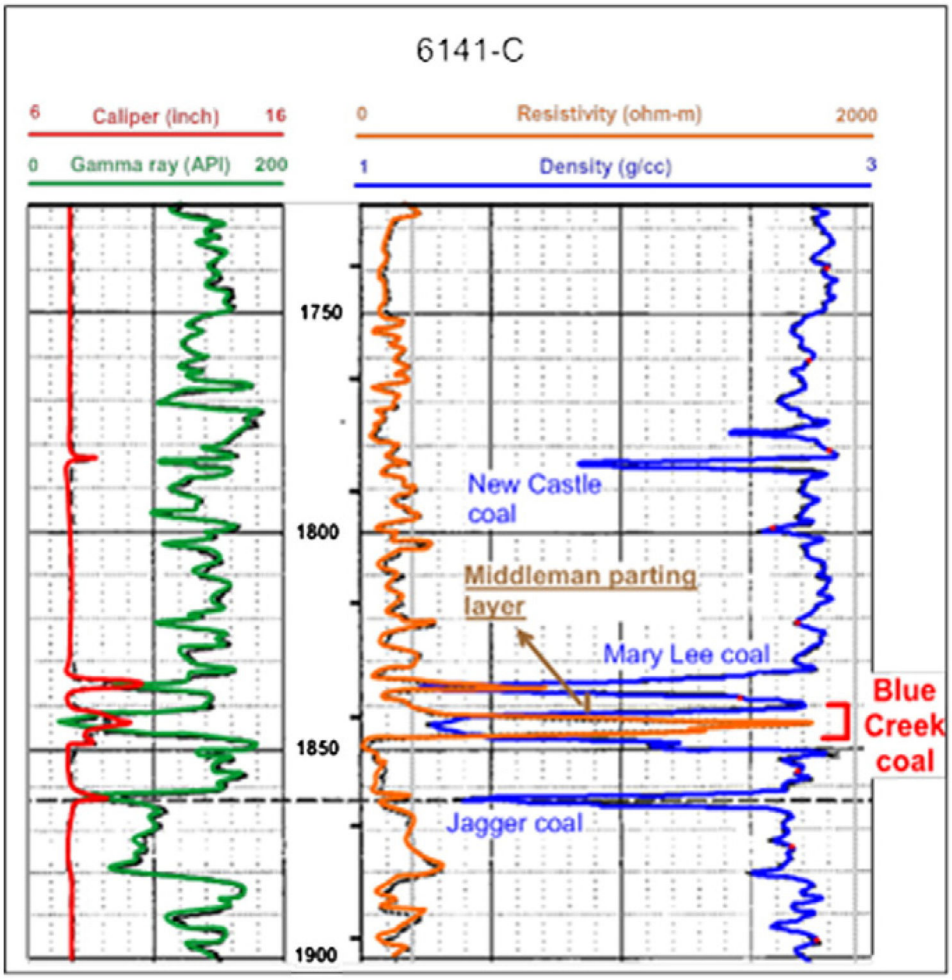


**Fig. 3.**

A typical well log response from the Mary Lee coal group. The figure shows the seams within the Mary Lee coal group and their approximate depth intervals within the study area. This particular log was recorded from well 6141-C, whose location within the study area is shown in Fig. 2.

Author Manuscript Author Manuscript Author Manuscript Author Manuscript

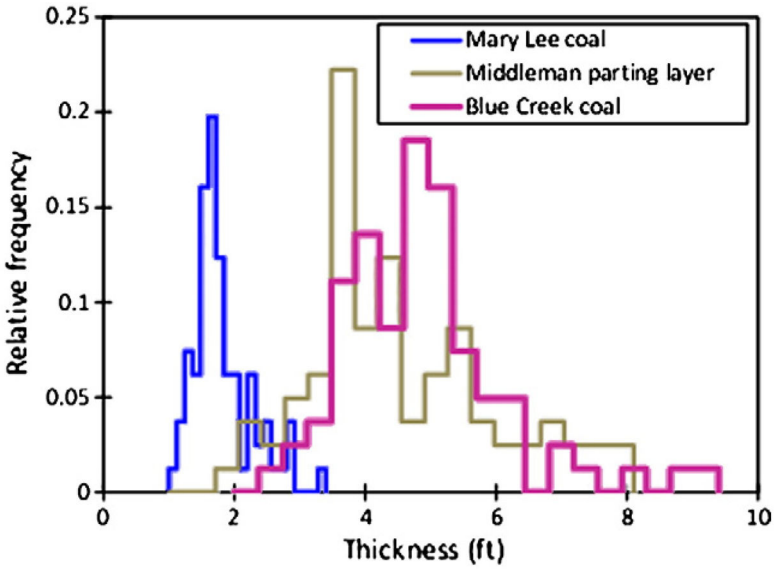


**Fig. 4.**

Thicknesses of Blue Creek and Mary Lee coal seams, and the Middleman parting layer (Fig. 3) within the study area shown in Fig. 2.

Author Manuscript Author Manuscript Author Manuscript Author Manuscript

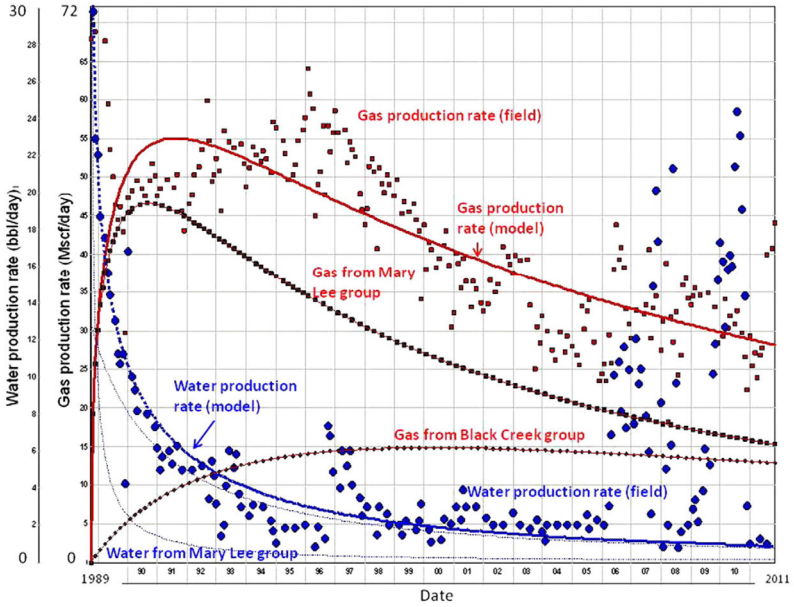


**Fig. 5.**

Example history matching results for 5603-C that was completed in two layers. Solid lines show the simulated data for gas and water production from each coal group for which local reservoir properties could be determined.

Author Manuscript Author Manuscript Author Manuscript Author Manuscript

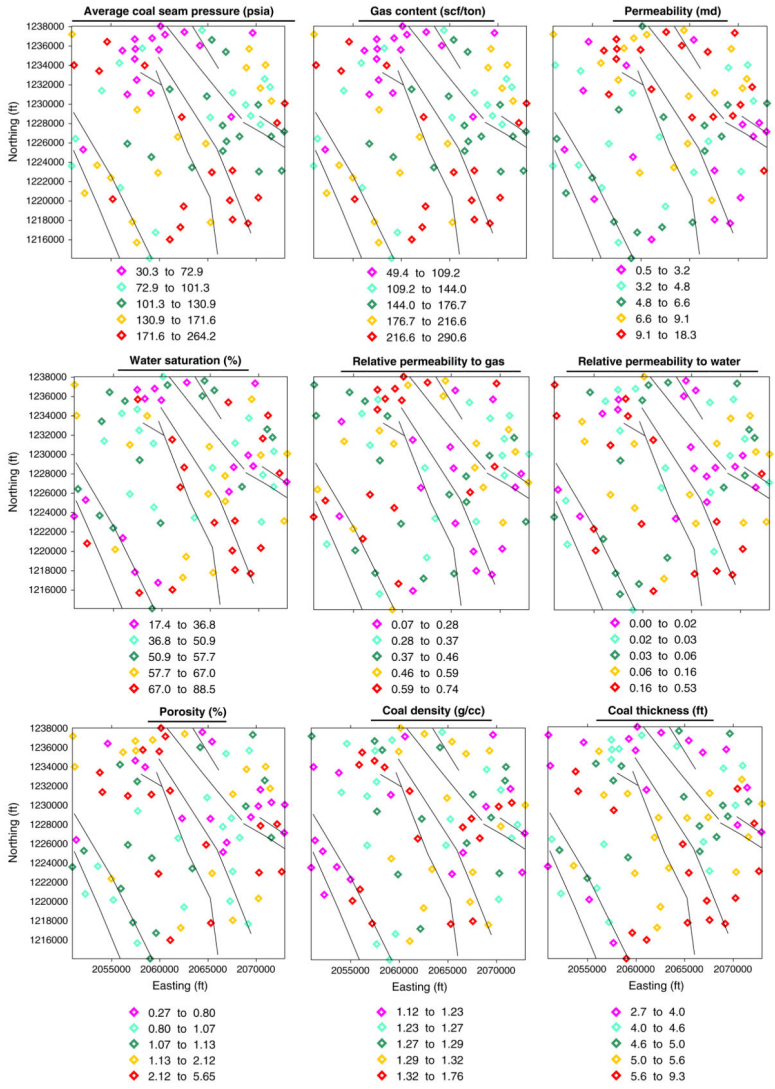


**Fig. 6.**

Spatial distributions of reservoir parameters estimated from the history matching study and from well logs. Values represent the condition of the Blue Creek seam in 2010. Solid black lines are the faults shown in Fig. 2 as well.

Author Manuscript Author Manuscript Author Manuscript Author Manuscript

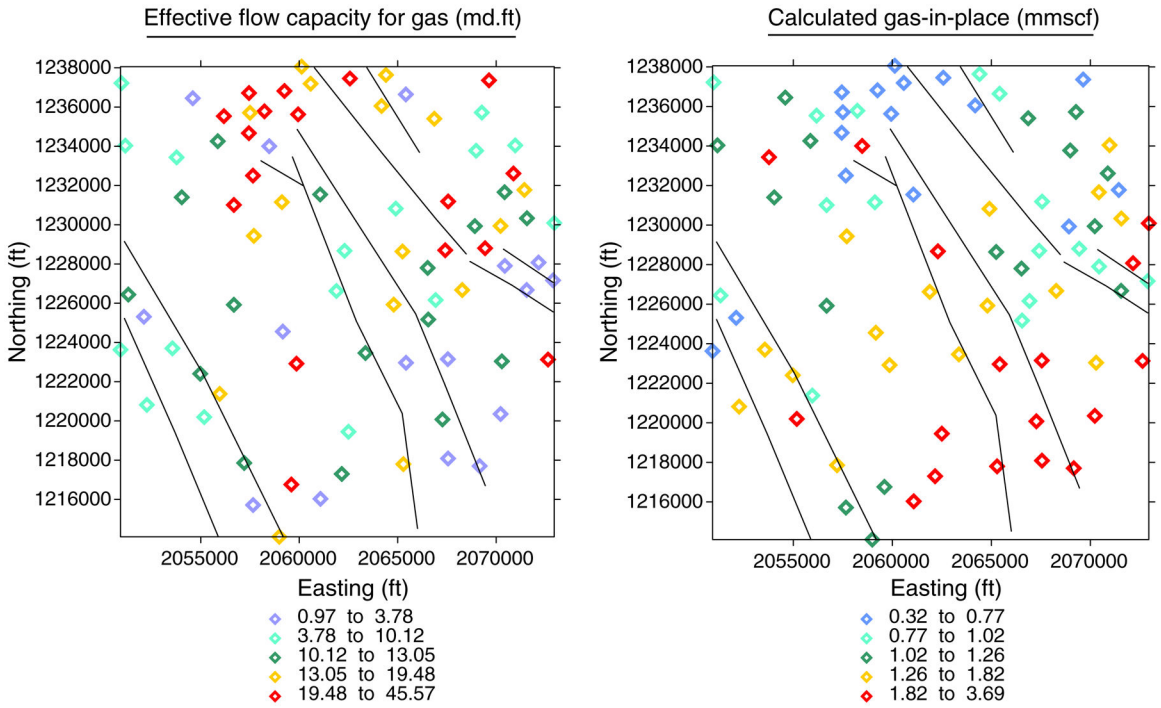


**Fig. 7.**

Spatial distributions of $k_{eff}h$ and GIP of the Blue Creek coal in 2010 at 81 vertical degasification borehole locations. The reported values for GIP were calculated for the area of wellbore cells, which was equal to 0.92 acres, of the geostatistical models that will be presented in upcoming sections.

Author Manuscript Author Manuscript Author Manuscript Author Manuscript

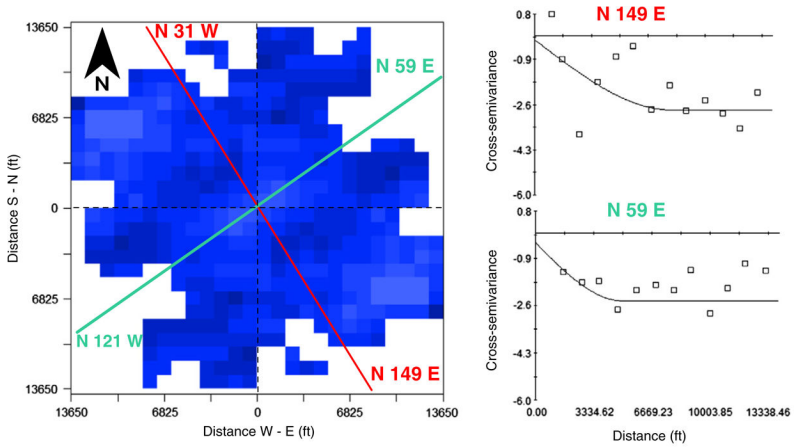


**Fig. 8.**

Cross-semivariogram map of $k_{eff}h$ and GIP (Fig. 7) and axes of major and minor anisotropies. Cross semivariograms shown on the right side of the map are along the N 149° E (major) and N 59° E (minor) directions shown on the map.

Author Manuscript Author Manuscript Author Manuscript Author Manuscript

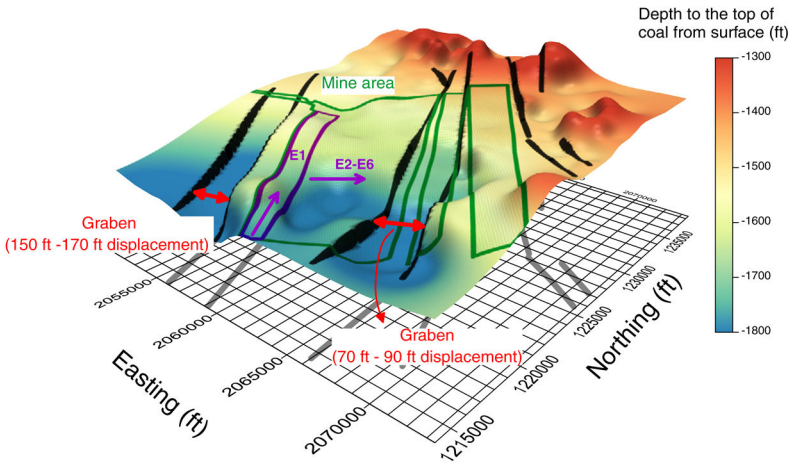


**Fig. 9.**

A three-dimensional representation of the depth to the top of the Blue Creek seam, with an outline of the mine area and the structural features due to faults.

Author Manuscript Author Manuscript Author Manuscript Author Manuscript

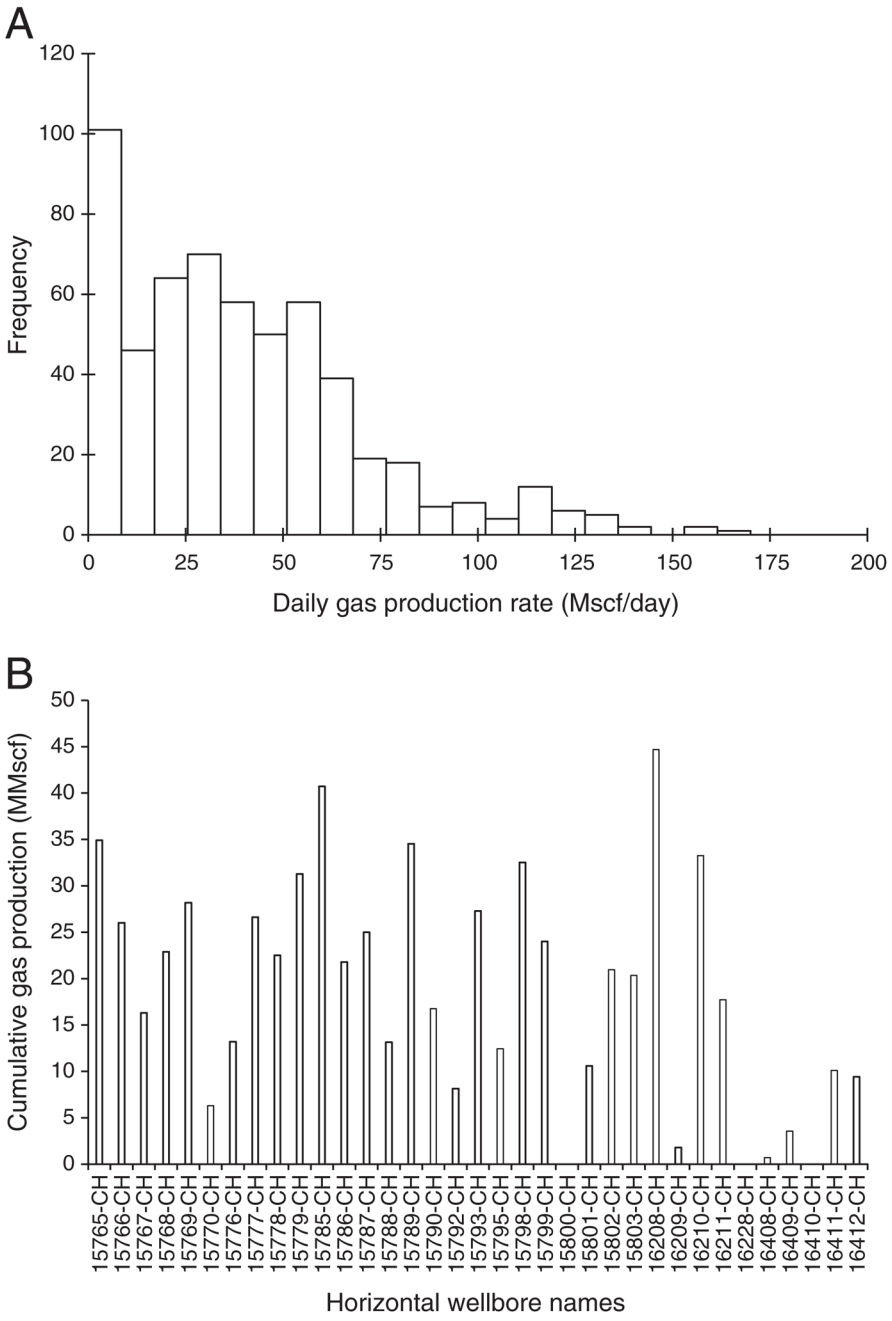


**Fig. 10.**

Histogram of average daily gas rates (A) and cumulative productions (B) recorded from all in-seam boreholes to date.

Author Manuscript Author Manuscript Author Manuscript Author Manuscript

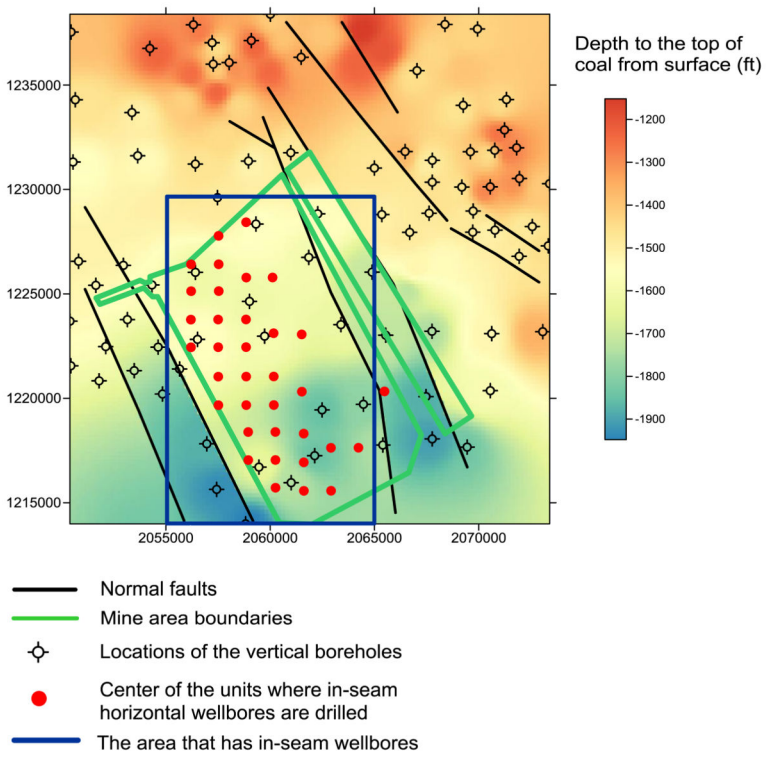


**Fig. 11.**
Plan view of the general mine area with well locations within.

Author Manuscript Author Manuscript Author Manuscript Author Manuscript

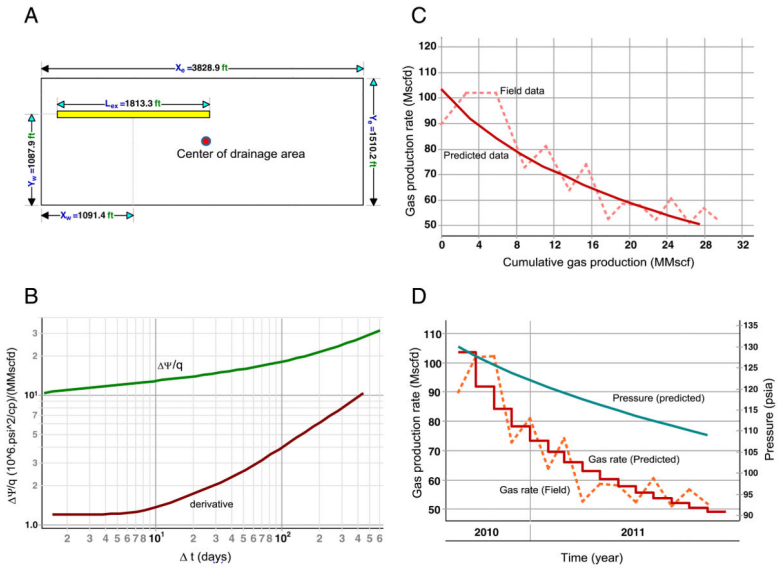


**Fig. 12.**

Results of the modeling for 15779-CH: Drainage area and the length and position of the effective horizontal well (A), type-curve results (B), and production data matches (C and D).

Author Manuscript Author Manuscript Author Manuscript Author Manuscript

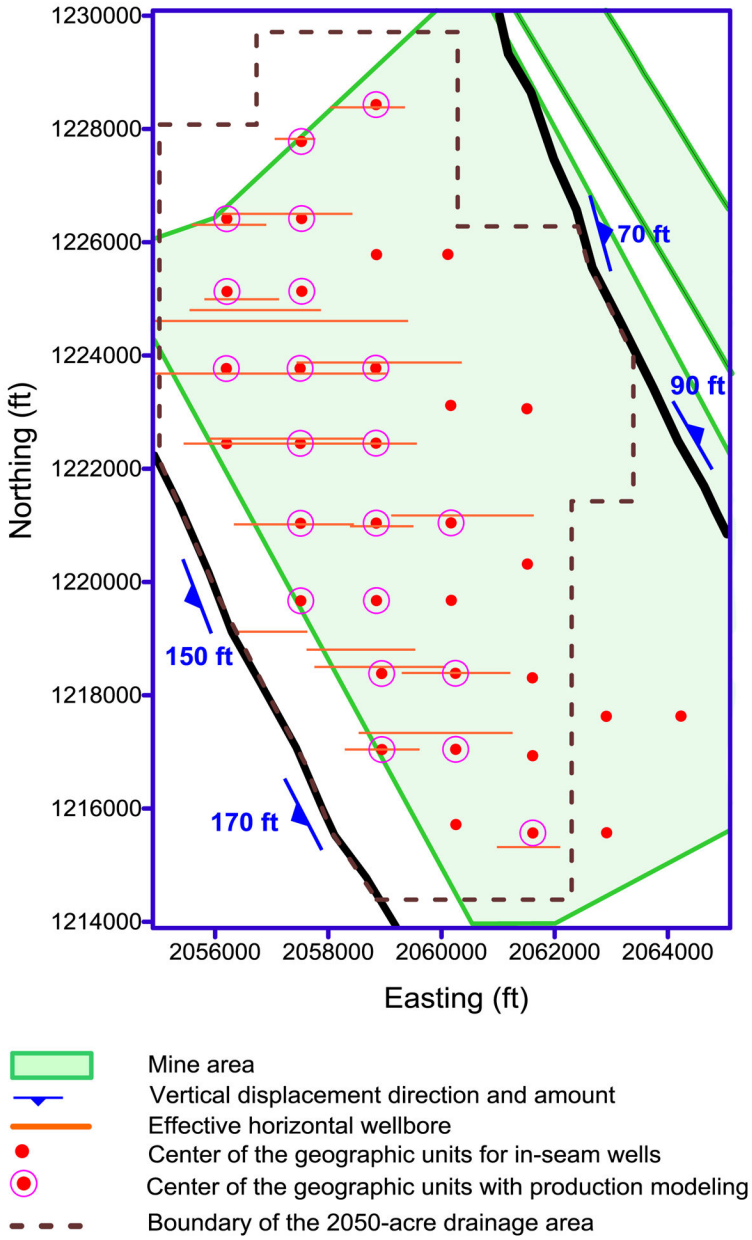


**Fig. 13.**

Locations of the effective horizontal wells in the main mine area and the boundary of the approximate effective drainage area.

Author Manuscript Author Manuscript Author Manuscript Author Manuscript

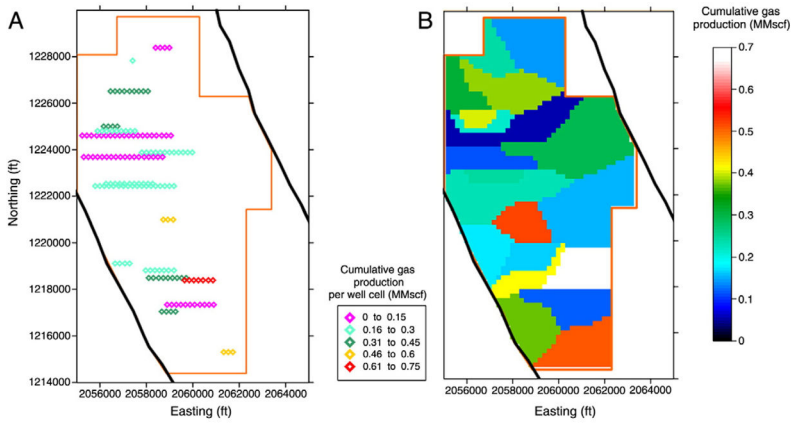


**Fig. 14.**

Cumulative gas production per cell collocated with effective well locations (A) and interpolation of this data based on nearest-neighbor approach (B) in the effective cumulative drainage area.

Author Manuscript Author Manuscript Author Manuscript Author Manuscript

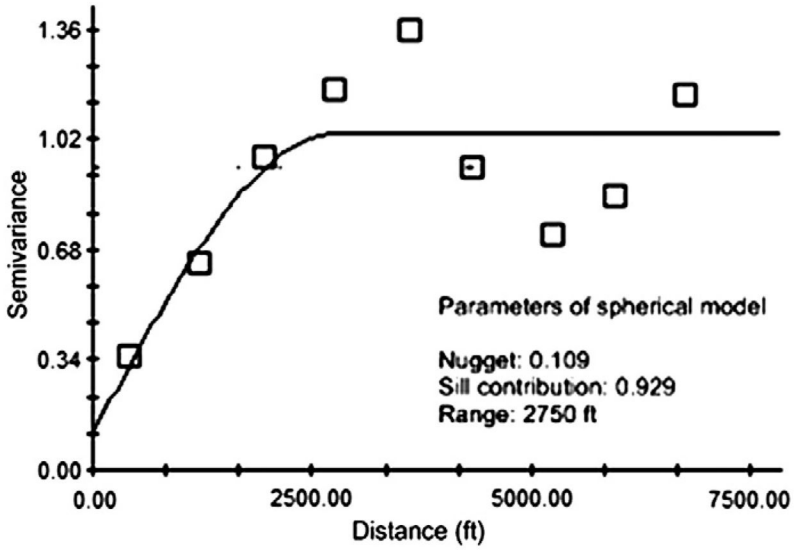


**Fig. 15.**
Omni-directional semivariogram of the spatial data shown in Fig. 14-A.

Author Manuscript Author Manuscript Author Manuscript Author Manuscript

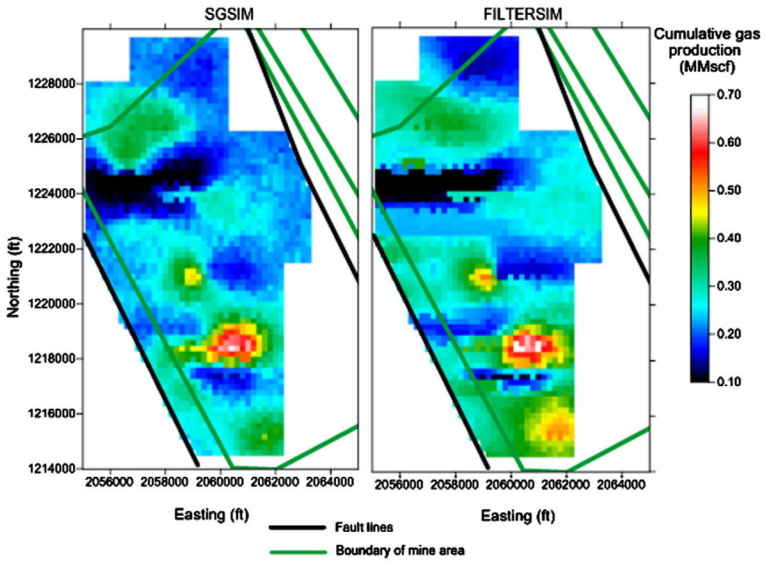


**Fig. 16.**

E-type maps of cumulative gas production by effective horizontal wells from the total drainage area.

Author Manuscript Author Manuscript Author Manuscript Author Manuscript

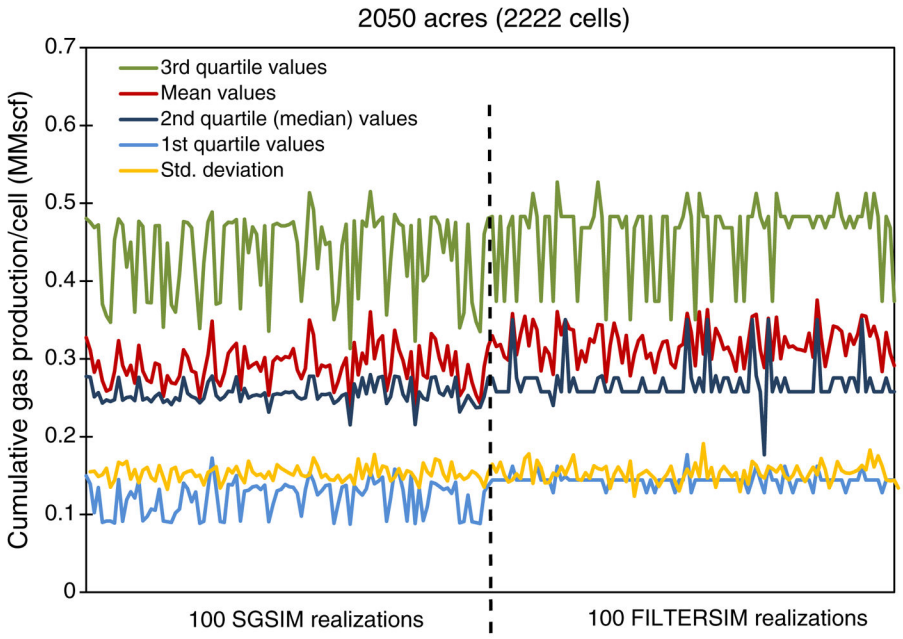


**Fig. 17.**

Comparison of basic statistical measures of cell values from individual realizations of SGSIM and FILTERSIM. Values in MMscf per 0.92 acre.

Author Manuscript Author Manuscript Author Manuscript Author Manuscript

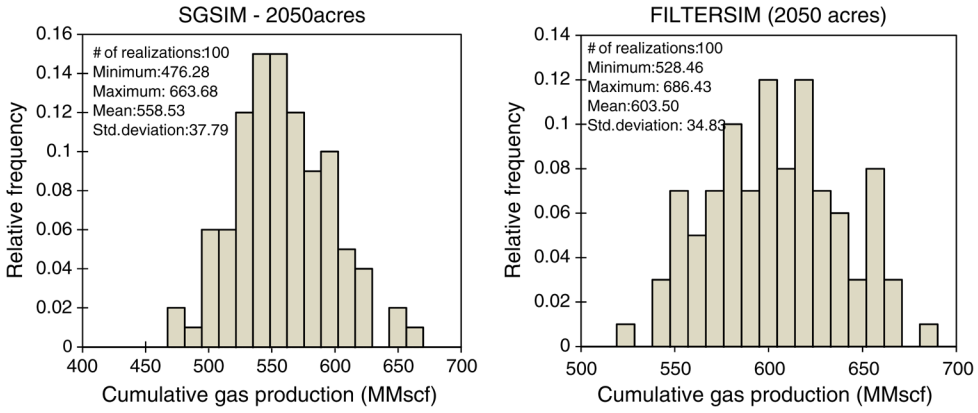


**Fig. 18.**

Histograms of cumulative gas productions from the 2050-acre drainage area based on 100 realizations of SGSIM and FILTERSIM.

Author Manuscript Author Manuscript Author Manuscript Author Manuscript

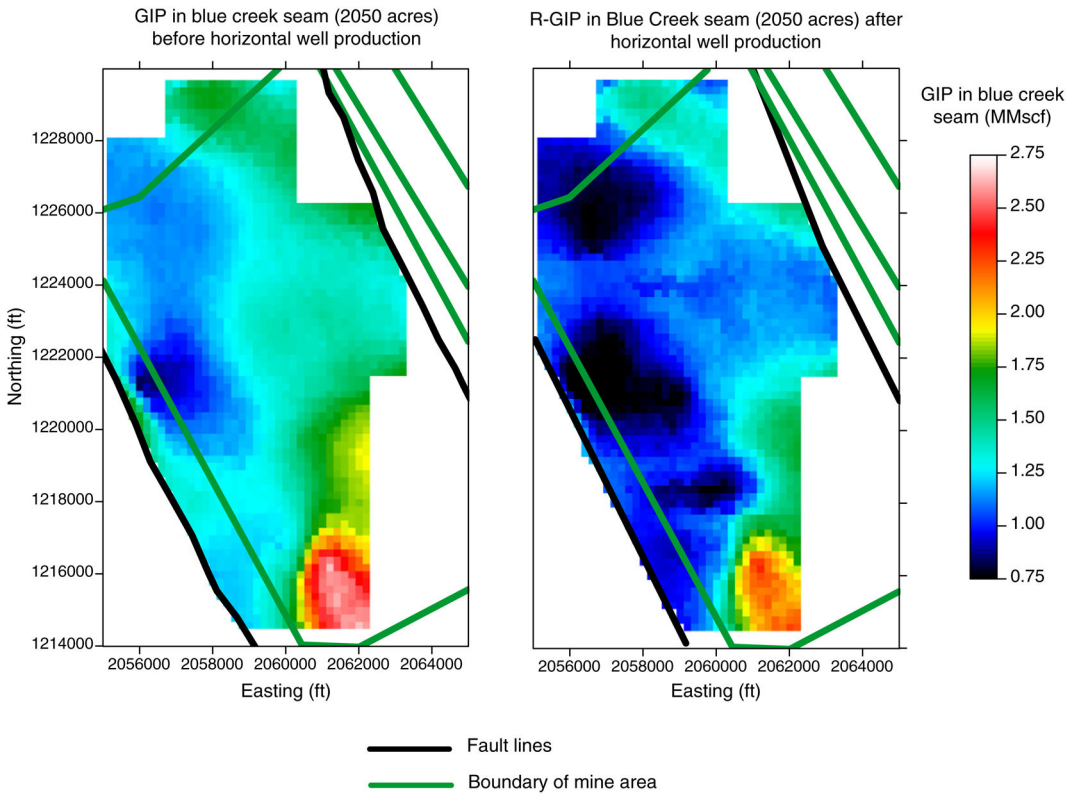


**Fig. 19.**

GIP and R-GIP E-type maps of the 2050-acre drainage area based on 100 realizations.

Author Manuscript Author Manuscript Author Manuscript Author Manuscript

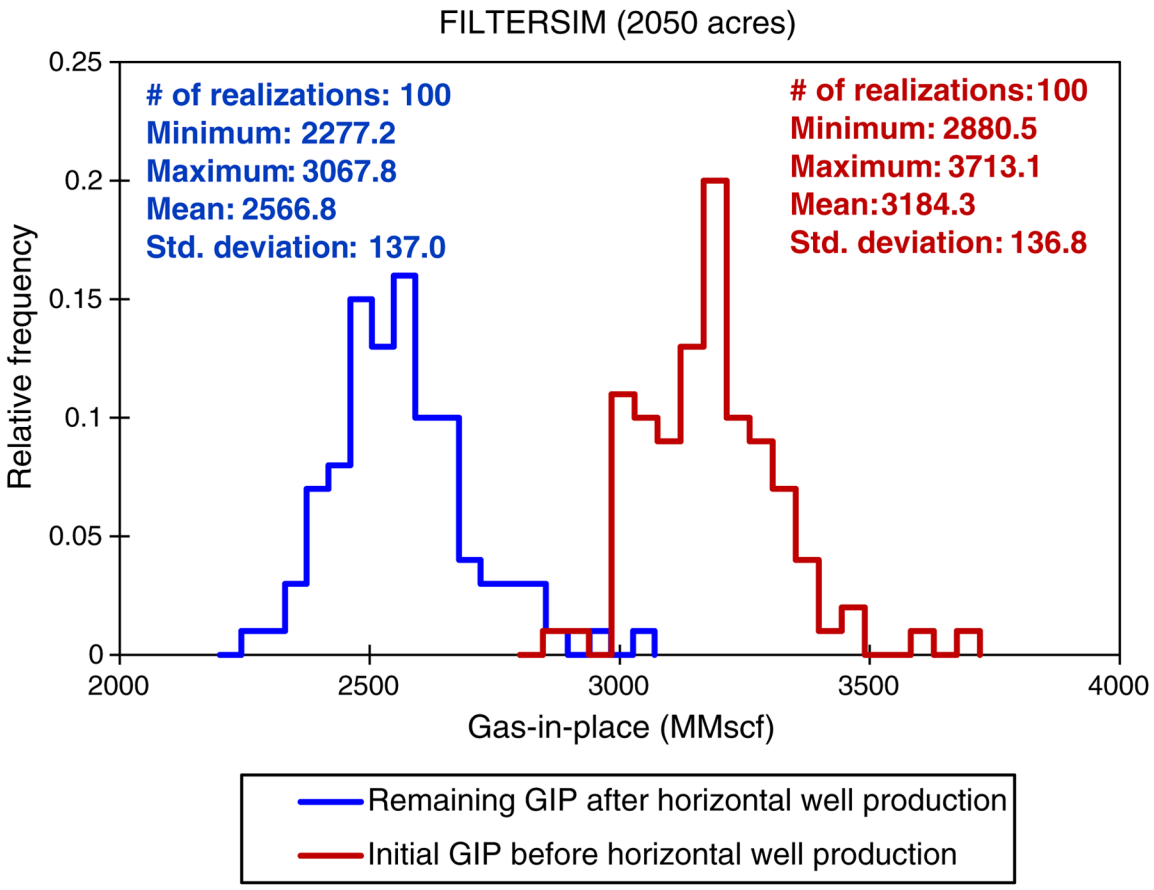


**Fig. 20.**
Relative frequency histograms of cumulative GIP and R-GIP values from realizations.

Author Manuscript Author Manuscript Author Manuscript Author Manuscript

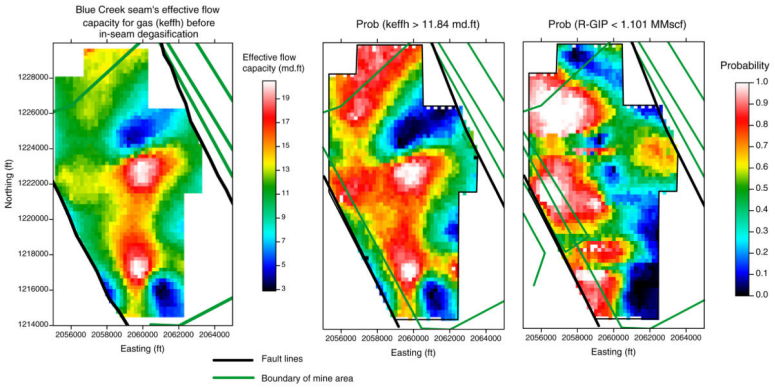


**Fig. 21.**

E-type map of $k_{eff}h$ and the probability maps of $k_{eff}h$ values higher than 11.84 md.ft, and R-GIP less than 1.101 MMscf per 0.92 acre.

Author Manuscript

Author Manuscript

Author Manuscript

Author Manuscript

**Table 1**

Compositional, petrographic and Langmuir properties of Blue Creek seam.

| | | |
|---|---|---|
| Dry-ash free composition (weight %) | Fixed carbon | 73.72 |
| | Volatiles | 26.28 |
| Ultimate and proximate analyses | Moisture | 1.26 |
| (as received) | Ash | 9.52 |
| (unit: weight %) | Fixed carbon | 65.71 |
| | Volatiles | 23.52 |
| | Heat of combustion (Btu/lb) | 13925 |
| | Carbon | 81.68 |
| | Hydrogen | 4.41 |
| | Nitrogen | 1.50 |
| | Oxygen | 0.20 |
| | Total sulfur | 1.44 |
| | Sulfatic sulfur | 0.69 |
| | Organic sulfur | 0.24 |
| | Pyritic sulfur | 0.51 |
| General petrographic Composition | Vitrinite (%) | 87.10 |
| | Liptinite (%) | 1.90 |
| | Inertinite (%) | 10.90 |
| Langmuir parameters (as received) | $V_L$ (scf/ton) | 791.10 |
| | $P_L$ (psia) | 455.10 |

Author Manuscript

Author Manuscript

Author Manuscript

Author Manuscript

**Table 2**

Composition analyses of the gas sample taken from the 11090-C vertical degasification well.

| **Gas composition from 11090-C** | |
|---|---|
| He | 0.0067 |
| $H_2$ | 0.0018 |
| Ar | 0.0181 |
| $O_2$ | 0.25 |
| $CO_2$ | 0.14 |
| $N_2$ | 1.08 |
| CO | 0 |
| $C_1$ | 98.49 |
| $C_2$ | 0.011 |
| $C_2H_4$ | 0 |
| $C_3$ | 0.001 |
| $iC_4$ | 0 |
| $nC_4$ | 0 |
| $iC_5$ | 0 |
| $nC_5$ | 0 |
| $C_{6+}$ | 0 |
| Specific gravity | 0.561 |
| $\delta_{13}C_1$ (‰) | −46.45 |
| Heat of combustion (Btu/Mscf) | 999.0 |

Author Manuscript Author Manuscript Author Manuscript Author Manuscript



**Table 3**

Univariate statistics based on 81 values of the Blue Creek coal reservoir parameters predicted by history matching analyses for 2010.

| | Pressure (psia) | Gas content (scf/t) | Permeability (md) | Relative permeability to gas | Relative permeability to water | Water saturation (%) | Porosity (%) | Formation vol. factor (rcf/Mscf) | Coal density (g/cc) | Coal thickness (ft) |
|---|---|---|---|---|---|---|---|---|---|---|
| # of wells | 81 | 81 | 81 | 81 | 81 | 81 | 81 | 81 | 81 | 81 |
| Minimum | 30.31 | 49.40 | 0.53 | 0.07 | 0.00 | 17.37 | 0.27 | 52.28 | 1.12 | 2.70 |
| Maximum | 264.19 | 290.57 | 18.30 | 0.74 | 0.53 | 88.44 | 5.65 | 468.39 | 1.76 | 9.30 |
| 1st Quartile | 77.03 | 114.52 | 3.75 | 0.30 | 0.02 | 41.15 | 1.01 | 91.38 | 1.25 | 4.10 |
| Median | 114.63 | 159.17 | 5.66 | 0.42 | 0.04 | 54.38 | 1.10 | 122.74 | 1.27 | 4.80 |
| 3rd Quartile | 153.25 | 199.29 | 8.10 | 0.53 | 0.10 | 64.10 | 2.05 | 183.47 | 1.30 | 5.30 |
| Mean | 121.99 | 161.45 | 6.24 | 0.42 | 0.08 | 53.01 | 1.46 | 147.75 | 1.27 | 4.87 |
| Std. dev. | 57.01 | 59.59 | 3.66 | 0.16 | 0.10 | 16.06 | 0.89 | 84.54 | 0.08 | 1.21 |

*Int J Coal Geol*. Author manuscript; available in PMC 2015 October 01.

Author Manuscript

Author Manuscript

Author Manuscript

Author Manuscript

**Table 4**

Univariate statistics based on 81 values of the $k_{eff}h$ and GIP (per 0.92 acre) in the Blue Creek for 2010.

| | **Effective flow capacity for gas ($k_{eff}h$) — md.ft** | **Gas-in-place in 0.92-acre cells (MMscf)** |
|---|---|---|
| # of wells | 81 | 81 |
| Minimum | 0.97 | 0.32 |
| Maximum | 45.57 | 3.69 |
| 1st Quartile | 4.66 | 0.82 |
| Median | 11.82 | 1.14 |
| 3rd Quartile | 17.62 | 1.62 |
| Mean | 12.78 | 1.30 |
| Std. dev. | 9.41 | 0.71 |

Author Manuscript Author Manuscript Author Manuscript Author Manuscript



**Table 5**

Horizontal wells of the drainage area shown in Fig. 13 and production modeling results. (OG: Oak Grove; BW: Brookwood).

| Well name | Field | Well length (ft) | Drainage area (acre) | Cumulative production (MMscf) | Production per well length (MMscf/ft) | Production per grid (MMscf/0.92 acre) |
|---|---|---|---|---|---|---|
| 15765-CH | OG | 2406.37 | 110.16 | 34.91 | 0.015 | 0.29 |
| 15766-CH | OG | 3618.94 | 104.67 | 26.01 | 0.007 | 0.23 |
| 15767-CH | OG | 3445.01 | 133.96 | 16.32 | 0.005 | 0.11 |
| 15768-CH | OG | 3960.38 | 389.60 | 22.90 | 0.006 | 0.05 |
| 15769-CH | OG | 2199.92 | 106.80 | 28.18 | 0.013 | 0.24 |
| 15770-CH | OG | | | 6.30 | | |
| 15776-CH | OG | 759.98 | 39.39 | 13.18 | 0.017 | 0.31 |
| 15777-CH | OG | 1832.06 | 64.10 | 26.63 | 0.015 | 0.38 |
| 15778-CH | OG | 701.53 | 51.53 | 22.53 | 0.032 | 0.40 |
| 15779-CH | OG | 1813.33 | 132.75 | 31.27 | 0.017 | 0.22 |
| 15785-CH | BW | 1690.96 | 37.20 | 40.73 | 0.024 | 1.01 |
| 15786-CH | BW | 493.13 | 38.52 | 21.77 | 0.044 | 0.52 |
| 15787-CH | BW | 1958.37 | 151.31 | 24.99 | 0.013 | 0.15 |
| 15788-CH | BW | 714.33 | 69.35 | 13.13 | 0.018 | 0.17 |
| 15789-CH | BW | 1446.56 | 193.39 | 34.55 | 0.024 | 0.16 |
| 15790-CH | BW | | | 16.75 | | |
| 15792-CH | OG | 837.80 | 20.10 | 8.13 | 0.010 | 0.37 |
| 15793-CH | OG | 2304.47 | 216.26 | 27.28 | 0.012 | 0.12 |
| 15795-CH | OG | | | 12.44 | | |
| 15798-CH | OG | 1817.51 | 72.60 | 32.52 | 0.018 | 0.41 |
| 15799-CH | OG | 1461.98 | 30.16 | 24.01 | 0.016 | 0.73 |
| 15801-CH | OG | 626.04 | 19.10 | 10.59 | 0.017 | 0.51 |
| 15802-CH | OG | | | 20.95 | | |
| 15803-CH | OG | | | 20.34 | | |
| 16208-CH | OG | | | 44.69 | | |
| 16209-CH | OG | 177.13 | 6.84 | 1.79 | 0.010 | 0.24 |
| 16210-CH | OG | | | 33.27 | | |
| 16211-CH | OG | | | 17.72 | | |

*Int J Coal Geol*. Author manuscript; available in PMC 2015 October 01.

Author Manuscript Author Manuscript Author Manuscript Author Manuscript



| Well name | Field | Well length (ft) | Drainage area (acre) | Cumulative production (MMscf) | Production per well length (MMscf/ft) | Production per grid (MMscf/0.92 acre) |
|---|---|---|---|---|---|---|
| 16409-CH | OG | | | 3.55 | | |
| 16411-CH | OG | | | 10.11 | | |
| 16412-CH | OG | 840.97 | 61.41 | 9.41 | 0.011 | 0.14 |
| Cumulative | | 35106.8 | 2049.2 | 656.9 | | |

*Int J Coal Geol*. Author manuscript; available in PMC 2015 October 01.

Author Manuscript

Author Manuscript

Author Manuscript

Author Manuscript

**Table 6**

Basic statistical measures of the cell values in E-type maps shown in Fig. 16. Values in MMscf per 0.92 acre.

| | SGSIM-E-type | FILTERSIM-E-type |
|---|---|---|
| # of cells | 2222 | 2222 |
| Minimum | 0.085 | 0.054 |
| Maximum | 0.674 | 0.733 |
| 1st Quartile | 0.208 | 0.221 |
| Median | 0.236 | 0.265 |
| 3rd Quartile | 0.284 | 0.316 |
| Mean | 0.251 | 0.272 |
| Std. dev. | 0.081 | 0.096 |

Author Manuscript

Author Manuscript

Author Manuscript

Author Manuscript

**Table 7**

Quantiles of cumulative gas productions based on the realizations of SGSIM and FILTERSIM and comparison with the measured production from the drainage area.

| Cumulative production quantiles (based on 100 realizations) | SGSIM (MMscf) | FILTERSIM (MMscf) |
|---|---|---|
| Q5 | 500.16 | 548.97 |
| Q50 | 559.19 | 601.36 |
| Q95 | 618.84 | 660.46 |
| E-type | 558.53 | 603.50 |
| Actual cumulative production in 2050-acre area (MMscf) | 656.9 | |

Author Manuscript

Author Manuscript

Author Manuscript

Author Manuscript

**Table 8**

Statistical measures of the cell value distributions in Q50 realizations of GIP and R-GIP.

| | GIP Q50 | R-GIP Q50 |
|---|---|---|
| # of cells | 2222 | 2222 |
| Minimum | 0.492 | 0.086 |
| Maximum | 3.689 | 2.575 |
| 1st Quartile | 1.115 | 0.816 |
| Median | 1.300 | 1.078 |
| 3rd Quartile | 1.434 | 1.282 |
| Mean | 1.404 | 1.125 |
| Std. dev. | 0.474 | 0.422 |

Author Manuscript

Author Manuscript

Author Manuscript

Author Manuscript

**Table 9**

Cumulative GIP and R-GIP values of E-type and Q5, Q50, and Q95 realizations.

| Quantiles | Initial GIP in 2050 acres before horizontal well production (MMscf) | Remaining GIP in 2050 acres after horizontal well production (MMscf) |
|---|---|---|
| Q5 | 3004.1 | 2399.1 |
| Q50 | 3187.0 | 2553.8 |
| Q95 | 3391.2 | 2815.1 |
| E-type (Fig. 19) | 3184.2 | 2566.8 |